Marine and Petroleum Geology 67 (2015) 30–56

Contents lists available at ScienceDirect

Marine and Petroleum Geology

journal homepage: www.elsevier.com/locate/marpetgeo

Research paper

Shallower structure and geomorphology of the southern Puerto Rico offshore margin

J.L. Granja Bruña [a, *], U.S. ten Brink [b], A. Muñoz-Martín [a, c], A. Carbó-Gorosabel [a], P. Llanes Estrada [a]

[a] Applied Tectonophysics Group, Departamento de Geodinámica, Universidad Complutense de Madrid, 28040, Madrid, Spain
[b] United States Geological Survey, Woods Hole, MA, 02543, USA
[c] Instituto de Geociencias, Consejo Superior de Investigaciones Científicas-Universidad Complutense de Madrid, Spain

ARTICLE INFO

Article history:
Received 4 November 2014
Received in revised form
1 April 2015
Accepted 17 April 2015
Available online 28 April 2015

Keywords:
Caribbean plate
Puerto Rico
Thrust belt
Accretionary system
Imbricate structure
Normal faults
Block tilting

ABSTRACT

Oblique convergence between the North American and Caribbean plates along the eastern Greater Antilles island arc has yielded the asymmetric Muertos thrust belt in the backarc region. Offshore south of Puerto Rico, this thrust belt disappears and is replaced by a succession of NE–SW- and E–W-trending deep basins and steep ridges that characterize the western Anegada passage, resulting in a complex deformation pattern. Using new high-resolution multibeam bathymetry and seismic reflection profiles, we studied the geomorphology and shallower structure of the southern Puerto Rico offshore margin. We have identified four morphotectonic provinces: the Puerto Rican sub-basin and Muertos trough, the Muertos margin, the insular shelf and the western Anegada passage. The Muertos margin province shows two distinct slope sub-provinces: the active Muertos thrust belt – which includes lower and upper thrust belts with distinct deformational styles and lateral continuity – and the shelf slope highly-incised by a dense canyon network. This network is disrupted by the Investigator fault zone consisting of a 130 km-long E–W-trending band of active extensional deformation. The Investigator fault zone shows differential surface expression caused by along-strike changes in the magnitude and distribution of the deformation, though this deformation is driven by a N–S-oriented extension. In the western Anegada passage province, the Whiting basin and Whiting and Grappler ridges are formed by large dip-slip normal faults driven by a NW–SE-oriented extensional regime. The western St. Croix rise shows a complex structure where the NE–SW-trending NW-dipping normal faults observed at the summit of the rise predate the E–W-bounding faults that could accommodate the extensional deformation at the Present. This study provides detailed observations on the active tectonic and sedimentary processes to help future studies assessing the natural resources and the seismic and tsunamigenic hazard in the Puerto Rico region.

© 2015 Elsevier Ltd. All rights reserved.

1. Introduction

Thrust belts are commonly built by a sequence of imbricate thrust slices forming a deformed sediment wedge along the subduction zone (e.g., Scholl et al., 1980; Davis et al., 1983). The forearc region of island arcs is often characterized by accretionary systems or thrust belts lying along the lower slope and perched basins occupying the upper slope region close to the arc (e.g., Aleutian arc, Holbrook et al., 1999; Nankai, Moore et al., 1990). However, at several places around the world, thrust belts have developed on both sides of island arcs (e.g., Java-Timor, Panama, Vanuatu and the northeastern Caribbean). In these localities, the overall vergence of the backarc or retroarc thrust belt is opposite to that of the forearc thrust belt. For example, in the northeastern Caribbean, a north-verging accretionary prism lies to the north of the eastern Greater Antilles arc (Hispaniola and Puerto Rico), whereas a S-verging thrust belt lies to the south (Fig. 1). GPS-derived velocities and the occurrence of large earthquakes suggest that significant convergence across the plate boundary can take place in the backarc thrust belt (Java-Timor; Genrich et al., 1996; Vanuatu; Lagabrielle et al., 2003). Therefore, the seismic hazard of backarc thrust belts should be considered (ten Brink et al., 2009).

* Corresponding author. Tel.: +34 913 944 832; Fax: +34 913 944 631.
E-mail address: jlgranja@geo.ucm.es (J.L. Granja Bruña).

http://dx.doi.org/10.1016/j.marpetgeo.2015.04.014
0264-8172/© 2015 Elsevier Ltd. All rights reserved.

The surface expression of the submarine active thrust systems is a sequence of long, narrow, sub-parallel anticline ridges (e.g., Cascadia, Flueh et al., 1998; Makran, Smith et al., 2012; Kukowski et al., 2001; Nankai, Gulick et al., 2004). The lateral and vertical growth and evolution of such accretionary systems are associated with a deformation pattern that controls the seafloor morphology and the dynamics of the sedimentary process along and across the slope margin (Underwood, 1991). The study of the morphology and subsurface structure of the submarine thrust belts and associated slope processes is a key to understand the active sedimentary and tectonic processes associated with compressive margins (e.g., Underwood and Moore, 2011; Smith et al., 2012). An understanding of such active processes allows characterization of the deformation pattern and provides a basis for predicting the distribution of faulting and the nucleation of earthquakes.

In the offshore northeastern Caribbean, studies of the shallower tectonic structure were mainly focused on the main boundary plate at the Puerto Rico trench where the North American plate obliquely subducts beneath the Caribbean plate (e.g., Grindlay et al., 2005a; ten Brink, 2005, Fig. 1). Until the beginning of the 21st century, there were only sparse seismic reflection profiles and GLORIA side-scan sonar data along the southern slope of eastern Hispaniola and Puerto Rico (i.e., Muertos margin; Fig. 1). These data helped to document the active underthrusting of the Caribbean plate's interior beneath the island arc along the Muertos margin as well as the active extensional tectonics in the western Anegada passage (e.g., Matthews and Holcombe, 1976; Ladd et al., 1977, 1981; Jany, 1989; Jany et al., 1990; Masson and Scanlon, 1991; Dillon et al., 1996). From 2004 the cooperative work undertaken by the U. S. Geological Survey and the Universidad Complutense of Madrid using high-resolution multibeam bathymetry and 2D seismic reflection yielded a good coverage of the Puerto Rico–Virgin Islands region (Carbó-Gorosabel et al., 2005, 2010; Andrews et al., 2014). These data allowed several studies to focus on the active tectonics, recent sedimentation and seismic hazard in the Puerto Rico trench and the Mona and Anegada passages (e.g., ten Brink et al., 2004; López-Venegas et al., 2008; Chaytor and ten Brink, 2010, 2014). Old reprocessed multichannel seismic reflection data and new multibeam bathymetry data were used to investigate the shallower structure of the western and central Muertos margin (Granja Bruña et al., 2009, 2014). However, the eastern region of the Muertos margin (i.e., southern Puerto Rico insular slope) has not been investigated using new high-resolution multibeam bathymetry and seismic reflection data.

The aim of the present study is to interpret the along- and across-strike variations of the geomorphology and shallower structure of the offshore Puerto Rico southern insular slope. To address our objective, we carried out a combined interpretation of new high-resolution multibeam bathymetry and a dense data set of mostly new seismic reflection profiles. This study provides detailed observations of the shallower structure in the eastern Muertos margin, completing the studies carried out in the western and central sectors of the margin (Granja Bruña et al., 2009, 2014) and in the western Anegada passage (Raussen et al., 2013; Chaytor and

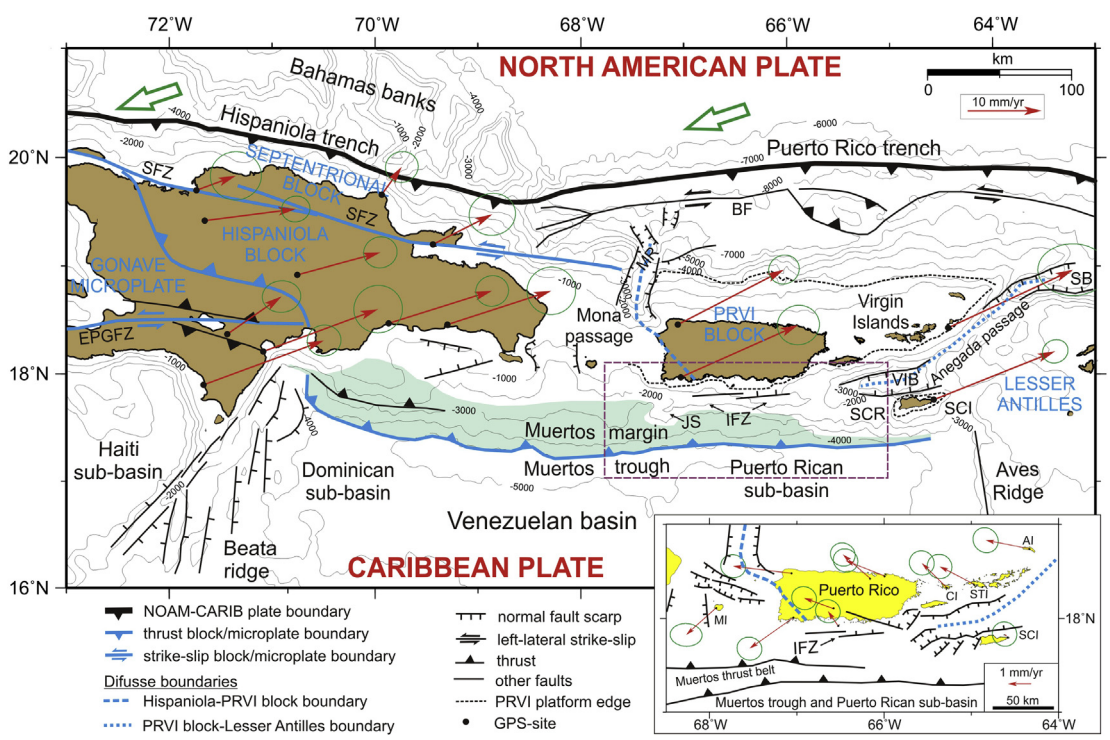

Figure 1. Contoured bathymetry map of the northeastern Caribbean showing a summarized tectonic setting. Isobaths based on satellite-derived bathymetry gridded at 1 arc-minute intervals (Smith and Sandwell, 1997) using the free software Generic Mapping Tools (GMT; Wessel and Smith, 1998). The purple dashed rectangle marks the study area. Thick green arrows show the relative convergence motion between the North American and the Caribbean plates. GPS-derived velocities with respect to the North American plate are shown with thin red arrows, the arrow length being proportional to the displacement rate (Manaker et al., 2008). Error ellipse for each vector represents two-dimensional error, 95% confidence limit. The thick blue dashed line marks the Hispaniola-PRVI block boundary as suggested by ten Brink and López-Venegas (2012). The green area shows the extension of the Muertos thrust belt (Granja Bruña et al., 2009, 2014, this study). NOAM = North American. CARIB = Caribbean. EPGFZ = Enriquillo-Plantain Garden fault zone. SFZ = Septentrional fault zone. BF = Bunce fault. SB = Sombrero basin. PRVI BLOCK = Puerto Rico–Virgin Islands block. VIB = Virgin Islands basin. MR = Mona rift. IFZ = Investigator fault zone. JS = Jaguey spur. SCR = St. Croix rise. SCI = St. Croix Island. The inset map shows GPS-derived velocities with respect to St. Croix Island (SCI), the arrow length being proportional to the displacement rate (ten Brink and López-Venegas, 2012). Error ellipse for each vector represents two-dimensional error, 95% confidence limit. MI = Mona Island. CI = Culebra Island. STI = St. Thomas Island. AI = Anegada Island. SCI = St. Croix Island. IFZ = Investigator fault zone. (For interpretation of the references to colour in this figure legend, the reader is referred to the web version of this article.)

ten Brink, 2014). We focus on the active tectonic and sedimentary processes in order to understand the complex deformation pattern and help provide a basis for future studies on the assessment of the natural resources and the seismic and tsunamigenic hazard in the Puerto Rico region (Huérfano et al., 2005; LaForge and McCann, 2005).

2. Tectonic setting

Along the E–W-trending Puerto Rico trench, the North American plate subducts under the Caribbean plate at a rate of 20.0 ± 0.4 mm/yr along an azimuth of $254 \pm 1^\circ$ (DeMets et al., 2010, Fig. 1). Subduction is thus highly oblique ($\geq 10^\circ$) to the plate boundary, resulting in strain partitioning and microplate tectonics along the eastern Greater Antilles island arc (e.g., Mann et al., 1995, 2002; Calais et al., 2002; ten Brink and Lin, 2004; Jansma and Mattioli, 2005; ten Brink and López-Venegas, 2012). Studies based on GPS-derived velocities, seismology and geological observations strongly suggest the existence of microplates and tectonic blocks in the northeastern Caribbean (Gonave microplate, Hispaniola block, Septentrional block and Puerto Rico–Virgin Island block in Fig. 1), but the boundaries of these tectonic units are not always well constrained because crustal seismicity is spatially diffuse. For example, a model of oblique intraarc extension with a complex interaction between bounding- and intra-rift faults was proposed for Mona Passage (Chaytor and ten Brink, 2010). In other cases, the interpretation of the structure is not yet fully understood mainly because of a very complex tectonic setting resulting from the superposition of several tectonic stages (e.g., Anegada passage; Fig. 1).

The Muertos trough marks the boundary between the Caribbean plate's interior and the eastern Greater Antilles (Fig. 1; e.g., Byrne et al., 1985; ten Brink et al., 2009). The Caribbean plate's interior is occupied by the extended Venezuelan basin that has been widely investigated by 2D seismic and DSDP surveys (e.g., Edgar et al., 1971; Diebold et al., 1981, 1999; Matthews and Holcombe, 1985; Mauffret and Leroy, 1999; Kroehler et al., 2011), allowing a good knowledge of the pelagic sedimentary section. The Muertos thrust belt is formed by the offscraping and accretion of pelagic sediments on the thickened oceanic crust of the Caribbean plate's interior and turbiditic sediments derived from the island arc (Granja Bruña et al., 2009). The Muertos thrust belt exhibits a southward transport direction and a progressive eastward narrowing, suggesting that the convergence rate decreases form W to E (Masson and Scanlon, 1991; Granja Bruña et al., 2009). However, the initiation age and convergence rate between the island arc and the Caribbean plate's interior are not well constrained. Model slip rates based on GPS-derived velocities on the Muertos thrust belt suggest a convergence of 3 mm/yr to the south of Hispaniola decreasing to 0.2 mm/yr to the south of Puerto Rico (Benford et al., 2012).

In the Puerto Rico region, the island arc is capped by the Puerto Rico–Virgin Islands carbonate platform (PRVI platform edge in Fig. 1). This platform is formed by an Oligocene to Recent sequence of terrestrial and shallow marine carbonates (van Gestel et al., 1998). The insular shelf was locally explored with single-channel seismic reflection surveys documenting several NE–SW- and E–W-trending faults, but the activity and kinematics were not well constrained (Denning, 1955; Garrison, 1969; Mann et al., 2005). Studies based on fault striation and terrace uplifting along the southern coast of Puerto Rico documented the existence of two phases of late Neogene extensional faulting (Mann et al., 2005): a first NE–SW-trending stage of Oligocene–Miocene age and a second NW–SE-trending stage of Post-Lower Pliocene to Quaternary ages. The upper insular slope off Puerto Rico shows a variable extension southward flanked by a steep shelf slope where the Investigator fault zone and the Jaguey spur are the main tectonic and morphologic features (IFZ and JS in Fig. 1; Case and Holcombe, 1980; LaForge and McCann, 2005).

The Anegada Passage is a deep-water basin and ridge province that forms a major crustal boundary between the Lesser and Greater Antilles island arc (Fig. 1). This passage consists of a NE–SW-trending broad band of deformation as a result of a combination of extensional and strike-slip faulting activity developed from Eocene to the Present (Jany et al., 1990). Extension certainly occurs but there is controversy related to the amount and sense of motion along suggested strike-slip faults as well as the orientation of the extensional deformation (Mann et al., 2005). GPS-derived velocities show the islands of Culebra and St. Thomas (CI and STI in the inset map of Fig. 1) moving to the NW relative to St. Croix Island at a rate of 1–1.5 mm/yr (ten Brink and López-Venegas, 2012), supporting a left-lateral transtensional model for the region (Gill et al., 1999; Raussen et al., 2013). The St. Croix rise (SCR in Fig. 1) is interpreted as an uplifted and tilted foot-wall block of a major N-dipping normal fault that has formed the Virgin Islands basin from post-Miocene ages (Bowles and Egloff, 1982). Dredging and diving on the northern flank documented Upper Cretaceous volcanic rocks composing the basement of the rise (Bouysse et al., 1985), while Lower Miocene shallow-water sediments located as deep as 2000 m suggested evidence of a large post-Lower Miocene subsidence in the northern flank that is still active (Jany et al., 1990).

Several regional models have been proposed to explain the transition between the Anegada passage and the Muertos thrust belt (Byrne et al., 1985; Masson and Scanlon, 1991; Larue and Ryan, 1998). These models suggest that just as the slip rate of the Muertos thrust belt decreases eastward, it must increase in the Anegada passage structures. The transition occurs along the Investigator fault zone (Fig. 1), which acts as an accommodating feature of the change in the tectonic style from N–S-oriented shortening at the Muertos margin to NW–SE-oriented extension in the Anegada passage. The Investigator fault zone was proposed to be an active strike-slip fault that accommodates left-lateral slip related to the convergence at the Muertos trough (van Gestel et al., 1998; Mann et al., 2005; LaForge and McCann, 2005).

3. Data

In the spring of 2005, an international research group headed by the Universidad Complutense of Madrid collected approximately 9500 km^2 of differential GPS navigated high-resolution swath bathymetry using the hull-mounted Kongsberg EM120 echo-sounder system installed on the Spanish R/V Hespérides (Carbó-Gorosabel et al., 2005). In the spring of 2006, the U.S. Geological Survey (USGS) collected approximately 18,000 km^2 of differential GPS navigated high-resolution multibeam swath bathymetry using the hull-mounted SeaBeam 2112 echo-sounder system installed on the NOAA Ship Ronald H. Brown (Andrews et al., 2014). Both datasets were merged allowing continuous seafloor coverage of the offshore Puerto Rico southern slope between 100 and 5100 m of water depth. The final edited data were gridded at a pixel resolution of 150 m in deep waters and at 50 m grid size at depths shallower than 1000 m (Fig. 2A; App. A and B). Complementing the study region in the Puerto Rican sub-basin, depth values were extracted from satellite-derived altimetry gridded at 2-minute intervals (Smith and Sandwell, 1997) and GEBCO bathymetric contours. Shallower regions and the insular shelf were complemented with data from different bathymetry datasets collected by Taylor et al. (2008).

Approximately 1030 km of multi-channel seismic (MCS) reflection profiles were collected across the southern Puerto Rico slope as part of a larger survey carried out by the USGS in October 2006 aboard the R/V Pelican (Fig. 2B). MCS profiles show coherent

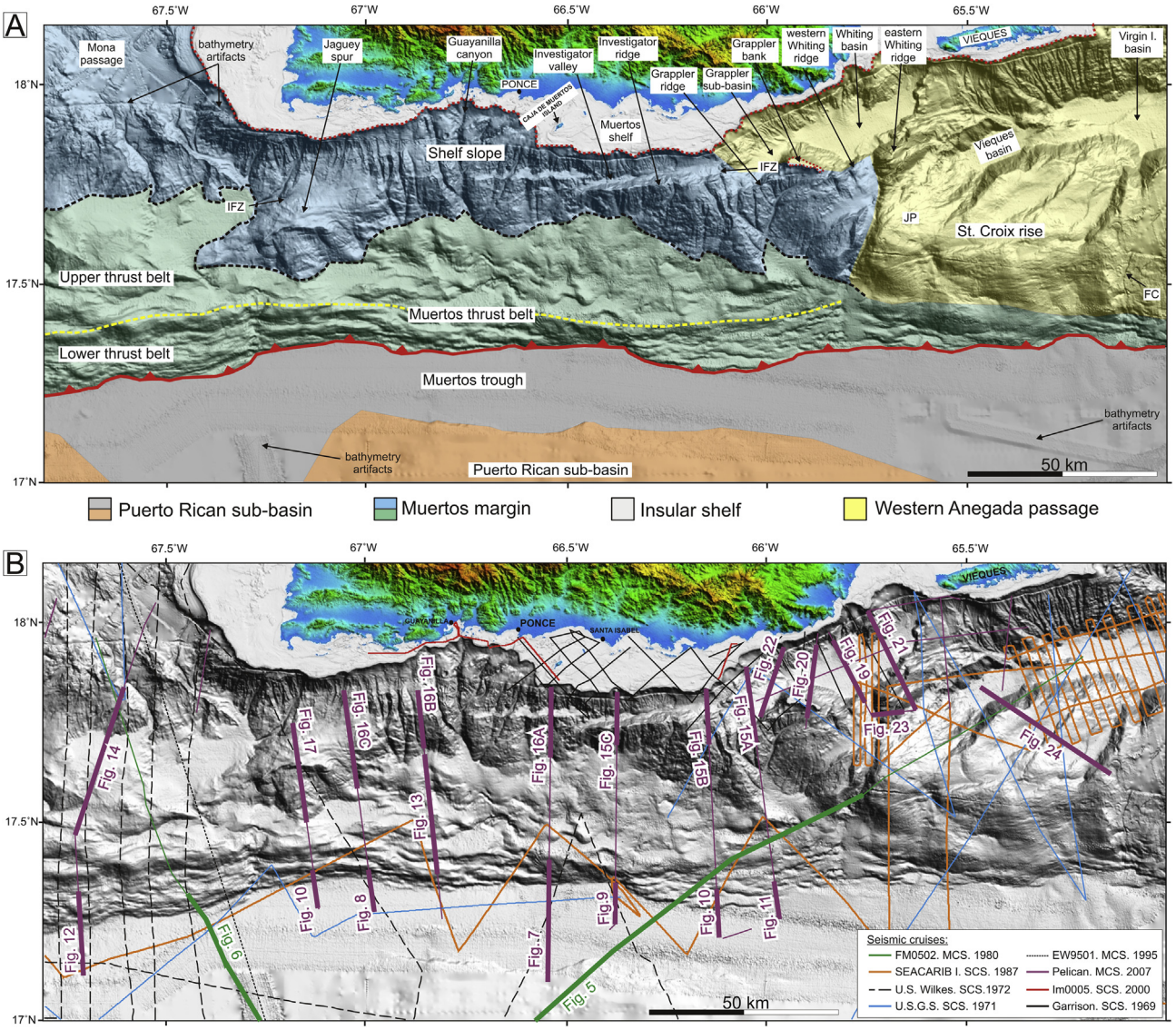

Figure 2. A) Digital Elevation Model (DEM) illuminated from the northeast derived from the compilation of different bathymetry data sets (For additional details see Appendixes A and B, and Taylor et al., 2008) showing the division into four morphotectonic provinces: Puerto Rican sub-basin-Muertos trough, Muertos margin, Insular shelf and Western Anegada passage. Different sub-zones of the provinces are: Muertos trough, Muertos thrust belt, Lower thrust belt, Upper thrust belt, Shelf slope, Jaguey spur, Muertos shelf, St. Croix rise. The thick black dashed line marks the concave slope break. The thick yellow dashed line marks the convex slope break. The thick red dotted line marks the shelf edge. IFZ = Investigator Fault Zone. JP = Jungfern passage. FC = Frederickted canyon. Multibeam data artifacts related to the overlapping among different swath data cruises are marked. **B)** DEM illuminated as in Figure 2A showing the location of the seismic reflection profiles data set used in this study. Heavier lines mark the sections of the seismic lines shown in this manuscript and are labeled with the figure number. SCS = Single-Channel Seismic. MCS = Multi-Channel Seismic. Seismic cruises are color coded by their acquisition year. (For interpretation of the references to colour in this figure legend, the reader is referred to the web version of this article.)

reflections up to a maximum of 1.5 sTWT, beyond which the limited source of power (GI guns of 105 and 35 cu.in) and receiver array (240 m-long and 24 channels) prevent reflections from the deeper section. Seismic processing included normal-moveout correction, band-pass filtering, common-depth point stacking and Stolt F–K post-stack migration. Additional old MCS profiles from the EW9501 cruise (1995), the IG1501 cruise (1976) and the FM0502 cruise (1980), as well as single-channel seismic (SCS) profiles from the WI932010 cruise (1972) and the SeaCarib-I cruise (1985), are used to complement the new seismic reflection data (Fig. 2B). For the insular shelf we used SCS data from the im0005 cruise (Grindlay et al., 2005b) and sparker profiling data collected by the USGS (Garrison, 1969). However, the quality of the SCS profiles is low because the presence of carbonate hard grounds yields high-amplitude seafloor reflections with limited sub-seafloor penetration, obscuring the sub-seafloor structure by multiples (Mann et al., 2005).

4. Interpretation of the shallower structure and morphology

Based on along- and across-strike morphological, structural and sedimentological criteria derived from the combined interpretation of the bathymetry and seismic data, we define the following morphotectonic provinces (Figs. 2A, 4A and B): the Puerto Rican sub-basin and Muertos trough, the Muertos margin, the insular shelf and the western Anegada passage.

4.1. The Puerto Rican sub-basin and Muertos trough province

4.1.1. Seafloor morphology

The Puerto Rican sub-basin is located in the northeastern corner of the Venezuelan basin and is bounded by the base of the Muertos margin (i.e., deformation front) and by the western slope of the Aves ridge (Fig. 1). The deeper area of the Puerto Rican sub-basin is

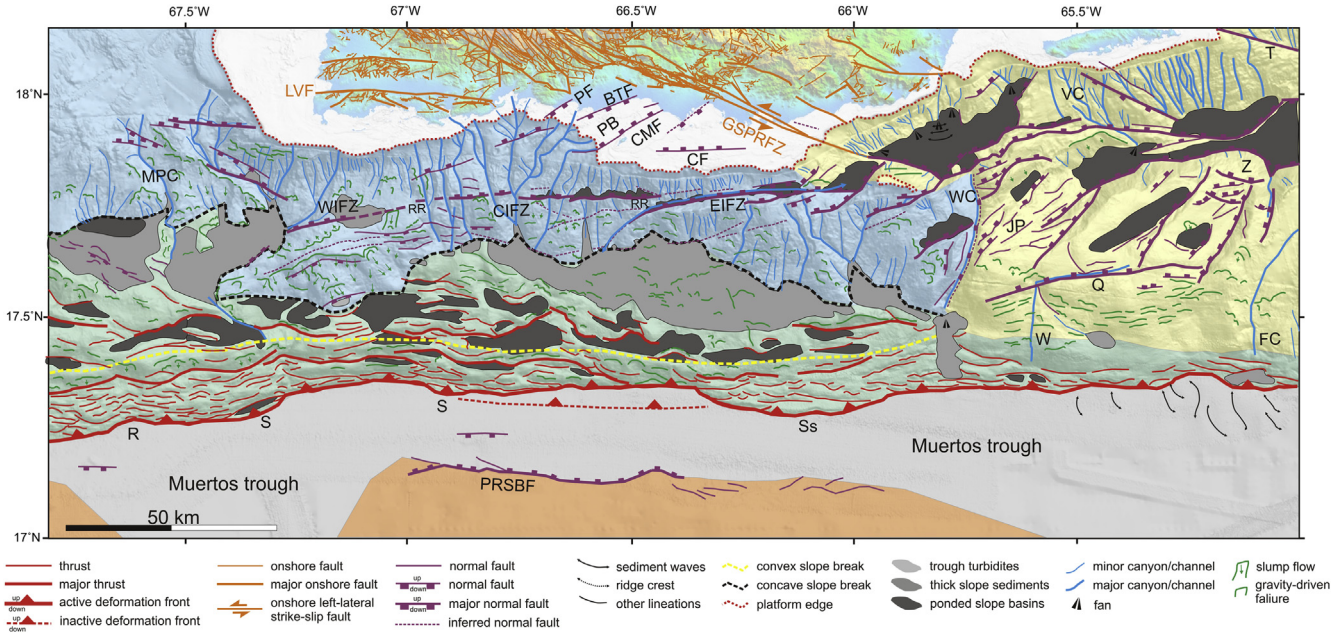

Figure 3. Regional morphotectonic interpretation. Faults picked from the seismic data and correlated along strike with the aid of swath bathymetry data. Thick orange lines mark the major onshore structures (GSPRFZ = Great Southern Puerto Rico fault zone; LVF = Lajas Valley fault). Thin orange lines show the faults mapped by Bawiec (1999). FC = Frederickted canyon. WIFZ = Western sector of the Investigator fault zone. CIFZ = Central sector of the Investigator fault zone. EIFZ = Eastern sector of the Investigator fault zone. PF = Ponce fault. BTF = Bajo Tasmanian fault. CMF = Caja de Muertos fault. CF = Central fault. MPC = Mona passage canyon. R = Recess. S = Salient in the deformation front. Ss = Salient in the deformation front referred in Section 4.1. JP = Jungfern passage. WC = Whiting canyon. VC = Vieques canyon. Z = Bench in the northern flank of St. Croix rise. PRSBF = Puerto Rican sub-basin fault. RR = Relay ramp. W = Canyon referred to in Section 4.4.3. Q = 080°-oriented fault in Section 4.4.3. T = possible source of the 1867 earthquake (Barkan and ten Brink, 2010) referred in Section 5.2. (For interpretation of the references to colour in this figure legend, the reader is referred to the web version of this article.)

the Muertos trough (Fig. 4B; App. A); a ≈700 km-long bathymetric depression formed along the base of the Muertos margin, from the Beata ridge in the west to the Aves ridge in the east. The Muertos trough reaches a maximum depth of 5580 m south of the Mona passage (Granja Bruña et al., 2009). In the study region the surface expression of the Muertos trough shows a smooth and featureless seafloor except local zones affected by active sedimentary and tectonic processes (e.g., sediment waves, fault scarps in Fig. 3; App. C). The existence of sediment waves is expected to be developed locally as a result of an important local supply of turbidite sediments (Wynn and Stow, 2002). The sediment waves are located at the mouth of Frederickted canyon (FC in Fig. 3). This canyon flows from the St. Croix island supplying sediments that contribute to the formation of the sediment waves. The roughly N–S-oriented strike of the crests and troughs of the sediment waves lying transversally to the E–W-tending deformation front suggests E–W-directed sediment transport along the trough.

The axial slope of the Muertos Trough increases at longitude 66°W (App. A), creating two distinct regions: a shallower eastern region with depths of 4200–5050 m and average axial slopes of 0.4°; and a deeper western region with an almost flat seafloor with depths of 5050–5150 m and average axial slopes of <0.1°. East of 67°W, the Muertos trough is confined on its south side by a bathymetric scarp, forming a ≈12–14 km-wide depression (Fig. 3). Southward of the bathymetric scarp the Puerto Rican sub-basin seafloor is shallower (4500–5000 m deep) and shows a rougher seafloor extending southwards into the Caribbean palte's interior (Apps. A and C). Core samples indicated that the Puerto Rican sub-basin seafloor is mainly composed of homogeneous carbonate pelagic muds and silts, and the Muertos trough of interbedded turbiditic and pelagic sediments (Forsthoff and Holcombe, 1983).

4.1.2. Sediment section

The sedimentary section of the Puerto Rican sub-basin and Muertos trough is being actively accreted along the deformation front of the Muertos thrust belt (Fig. 4A and B). The sedimentary sequence of the Puerto Rican sub-basin consists of sediments from Coniacian (ages and lithology determined by correlation with the 146/149 and 150 DSDP sites; e.g., Edgar et al., 1971, 1973; Matthews and Holcombe, 1985; Driscoll and Diebold, 1999; Kroehler et al., 2011) to recent times lying conformably over the top of the upper volcanic sequence of the Caribbean oceanic crust (Mauffret and Leroy, 1999, Fig. 5). The top of the upper volcanic sequence is marked by a highly-reflective and smooth seismic horizon (i.e., B" horizon; Figs. 5 and 6). The B" seismic horizon was correlated with sills of Upper Cretaceous tholeitic basalts intruding carbonate pelagic sedimentary rocks of the Coniacian (Edgar et al., 1973). The sedimentary section of the Puerto Rican sub-basin consists of a sequence of relatively constant thickness (~1 sTWT) with two sub-parallel and highly-continuous seismic horizons (Matthews and Holcombe, 1985): the A″ horizon (a siliceous limestone and chert unit dated as Middle Eocene) and the α horizon (an interface between marls and clays dated as Lower Miocene). The sedimentary section dips gently to the north and is onlapped and buried by a wedge-shaped sequence of ponded horizontal turbidite beds deposited along the Muertos trough (Figs. 5 and 6). The thickness of this undeformed wedge is locally up to 0.5 sTWT (Fig. 5), and decreases progressively southward and northward, onlapping and probably interfingering with the supra-α section of the Puerto Rican sub-basin and with the deeper tilted turbiditic layers near the deformation front respectively. The absence of any distinctive channel system along the trough seafloor and the horizontal disposition of the turbidite beds suggest that successive sheet-flow turbidites were the dominant sedimentation mechanism

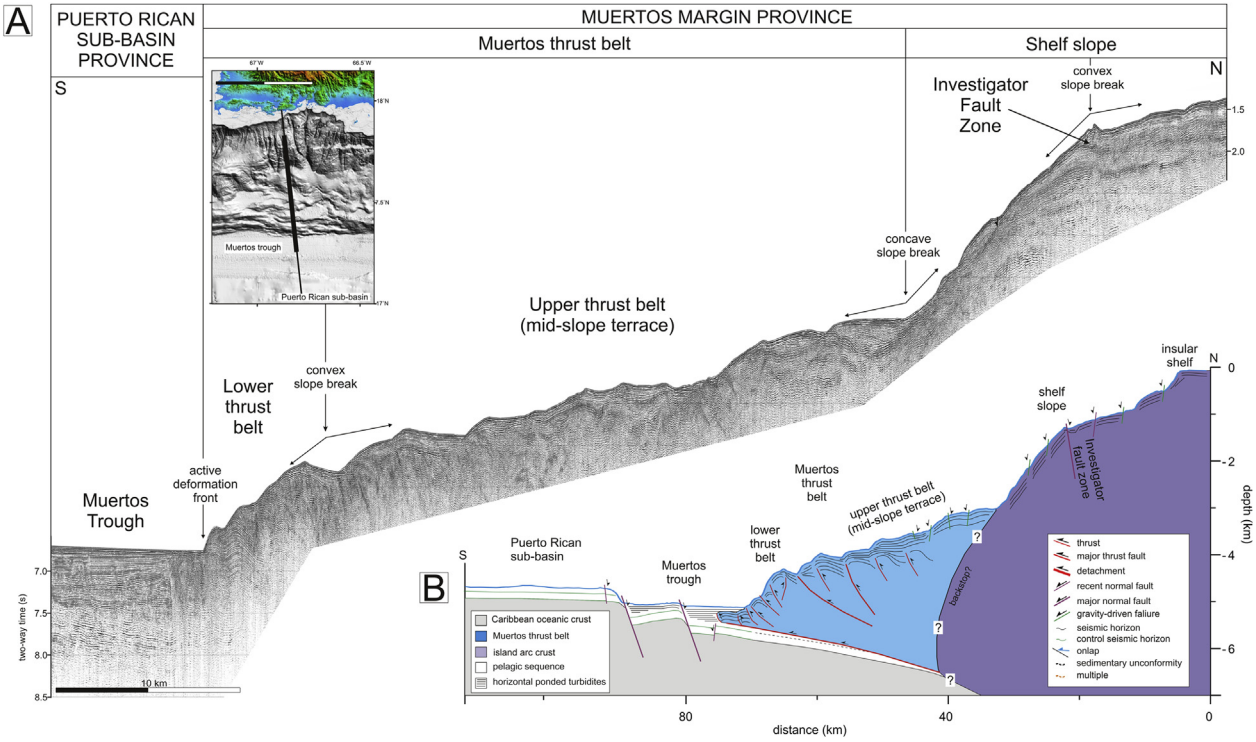

Figure 4. **A**) Post-stack migrated multi-channel seismic (MCS) profile. See location in the inset map V.E. is 6.0× on the seafloor. The inset map shows a DEM illuminated from the northeast showing the location of Figure 4A (thick solid black line) and B (thin solid black line). **B)** Schematic cross-section of the Muertos margin deduced from this study. The bathymetric profile was extracted from the DEM of Figure 2A. See location in the inset map of Figure 4A.

(Underwood, 1991). The depocenter location varies along strike related to changes in the balance between the rate of deformation and rate of sediment input. The depocenter could be located close to the deformation front or located in the axial zone of the Muertos trough basin (current depocenter in Figs. 5 and 6).

4.1.3. Shallower structure

Close to the Muertos trough, the top of the Caribbean oceanic crust (i.e., upper volcanic sequence) and the sedimentary section are broken over a short distance by numerous normal faults (Figs. 5 and 7). Faults offset the top of the oceanic basement and lower sedimentary layers, and only occasionally some fault propagates the upsection, deforming the seafloor locally (Figs. 3 and 7). Fault activity has yielded block tilting and an overall subsidence, which results in a deepening of the oceanic crust and an increase in the accommodation space of the basin formed in Muertos trough (Figs. 5 and 7). However, the faulting and block tilting process seems to be inactive because recently-ponded sediments are burying the faults (Figs. 7 and 8). Similar faulting pattern was documented in the central sector of the Muertos trough and interpreted as a response to the overburden yielded by the differential volume of accreted material in the Muertos thrust belt (Granja Bruña et al., 2009). The thickness of the Puerto Rican sub-basin section (i.e., B″- α interval) does not show lateral variation (or folding) in the proximity of the faults, suggesting that the block tilting started at least after Lower Miocene (α horizon). The continued onlap of the ponded sediment layers over the underlying sediment sequences related to thrust belt loading suggests that subsidence in the trough has continued at least from Lower Miocene (α horizon) until the Present (Fig. 7).

One major N-dipping normal fault located ≈20 km southwards from the deformation front breaks the seafloor (Puerto Rican sub-basin fault; PRSBF in Figs. 3 and 7). It has a large dip-slip displacement and forms a sinuous bathymetric scarp in map view oriented sub-parallel to the deformation front. This exposed fault scarp is observable along 60 km and has a maximum height of 380 m that decreases progressively along strike, being replaced by minor faults and finally buried by the horizontal trough sediments (buried PRSBF in Figs. 5 and 6). The fault offsets the A″ and α horizons by 0.3 sTWT, but the dip-slip throw decreases progressively upsection (Fig. 7). The well-preserved bathymetric scarp suggests that this fault could be a recent feature accommodating the greatest part of the deformation, but there is no evidence of recent deformation/folding in the adjoining horizontally-ponded sediments. This scarp acts as a topographic barrier that has prevented the turbidite spreading more southward over the Puerto Rican sub-basin. Where the scarp height diminishes along strike, the horizontal turbidite layers extend further southwards onlapping gentle northward-dipping sediment beds of the Puerto Rican sub-basin (Fig. 6). Growth faults are well identified in the turbiditic layers but do not break the seafloor (inset in Fig. 8). Locally growth faults are rooted by vertical zones devoid of coherent reflections, because they are possibly nucleated in deep faults related to block tilting. Although the origin of such faults could be related to the overburden of the accreted material in the thrust belt as in the central Muertos Margin (c.f., Granja Bruña et al., 2009), here in the south of Puerto Rico this process seems to be inactive.

4.1.4. Sediment accretion

The seismic horizons A″, B″ and α of the Puerto Rican sub-basin can be outlined northward beneath the turbidite wedge of the Muertos trough and beneath the deformed wedge of the Muertos thrust belt (Figs. 5 and 6). The thick and highly-deformed sediment section in the thrust belt prevents the identification of deeper structure and stratigraphy north of the deformation front. The

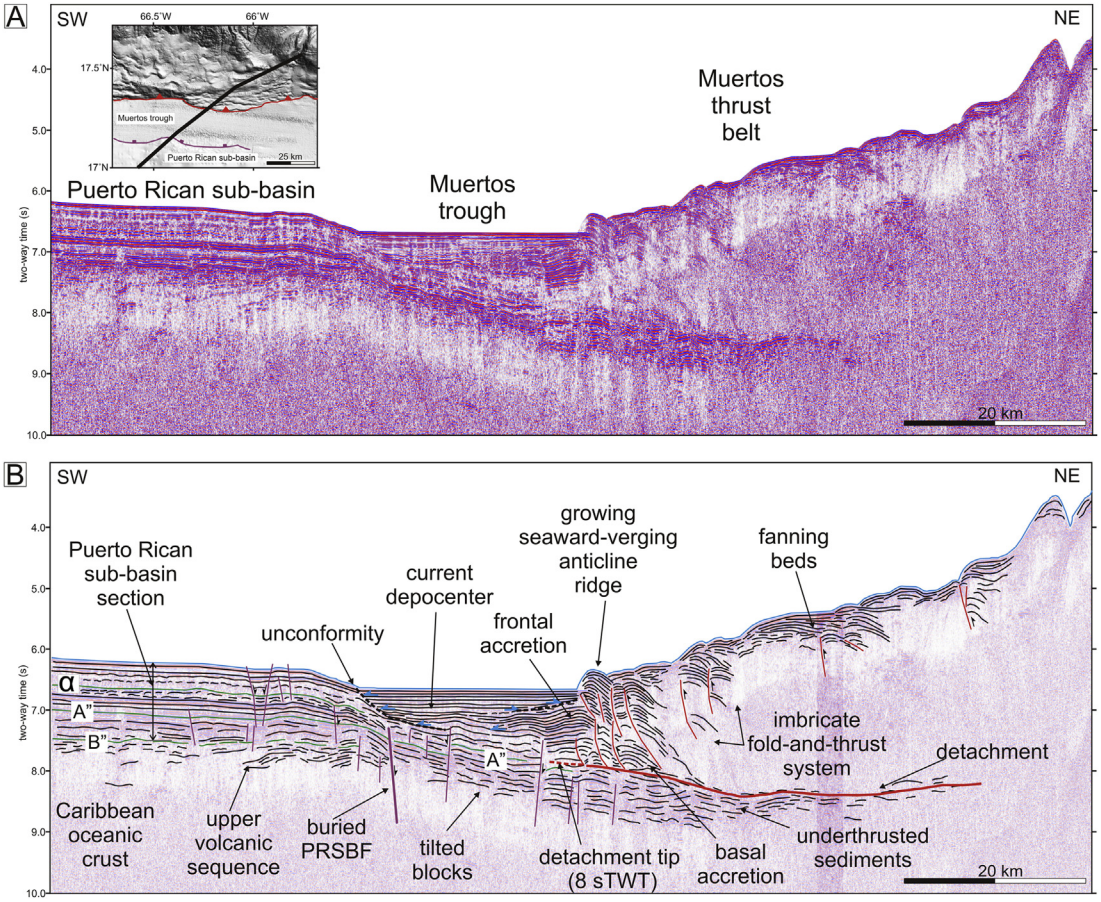

Figure 5. A) Stacked MCS profile. See location in the inset map. V.E. is 9.0× on the seafloor. **B)** Line drawing interpretation. See Figure 4B for legend. PRSBF = Puerto Rican sub-basin fault.

overthrusted sub-horizontal horizons of the Puerto Rican sub-basin form an angular unconformity with the overlying steeply-dipping reflectors of the accreted sediments and define a gentle northward-dipping detachment. This detachment can be traced beneath the Muertos thrust belt up to ≈25–30 km northwards from the deformation front (Fig. 5). This extension is similar to the extension observed in the central and western Muertos margin (Granja Bruña et al., 2009, 2014) and roughly coincides with the northward termination of the accretionary system and the start of the shelf slope sub-province (Fig. 2A). The detachment marks the decoupling level between the sediment that is offscraped and added to the thrust belt and the material that is carried northward and overthrusted beyond the deformation front (Fig. 4B). The detachment allows the compressive deformation to migrate southwards, deforming and tilting progressively southward the horizontal horizons of the turbidite wedge by means of successive fault-propagation folds (Figs. 9, 10 and 11). Each successive fault-propagation fold is inferred to connect at depth with the detachment, defining a thin-skin tectonic style (Figs. 5 and 12). The detachment propagates southwards approximately between A″ horizon and the base of the turbidite wedge (Figs. 5 and 7). Hence, the horizontal turbiditic sediments of the Muertos trough basin are offscraped and added to the thrust belt mainly by frontal accretion. On the other hand, most of the pelagic sediments of the Puerto Rico sub-basin are progressively offscraped and are added to the thrust belt through basal accretion (Fig. 5).

The active deformation front is formed by the growing anticline ridges located along the sinuous roughly E–W-trending base of the insular slope (Figs. 3 and 4). These anticline ridges are the seafloor expression of active frontal fault-propagation folds (Figs. 9 and 10). It would result feasible that some thrust faults coring the frontal propagation folds were formed by the inversion of the growth faults developed within the turbidite wedge, but seismic section do not provide enough detail. Locally, seismic data show the frontal fault-propagation folds buried by horizontal beds of turbidites and do not coincide with the base of the insular slope (Figs. 7 and 9). This fact suggests that the active deformation front changed its position relative to the accretionary system over time; it is now at the base of the insular slope but there were previous stages where it was located more southwards (inactive deformation front in Fig. 3). This fact suggests that where the frontal fault-propagation folds are buried by horizontal turbidite layers, the southward migration of the compressive deformation is not active. Changes in the position of the active deformation front are commonly related to changes in the detachment depth, resulting in a differential volume of sediments accreted (e.g., Marshak et al., 1992; Calassou et al., 1993; Marques and Cobbold, 2002). The changes in the detachment depth are a result of along-strike variation in the structure of the overthrusted plate (i.e., frequency and size of faulting, basement highs) and of the differential sediment input to the turbidite wedge (Figs. 1, 5 and 11). A deeper detachment implies a larger amount of sediments to be accreted and, therefore, an increase in the southward migration of the deformation front. Overthrusted basement highs of igneous origin in the central and western Muertos margin were identified and interpreted as the cause of the sinuous deformation front (Granja Bruña et al., 2009,

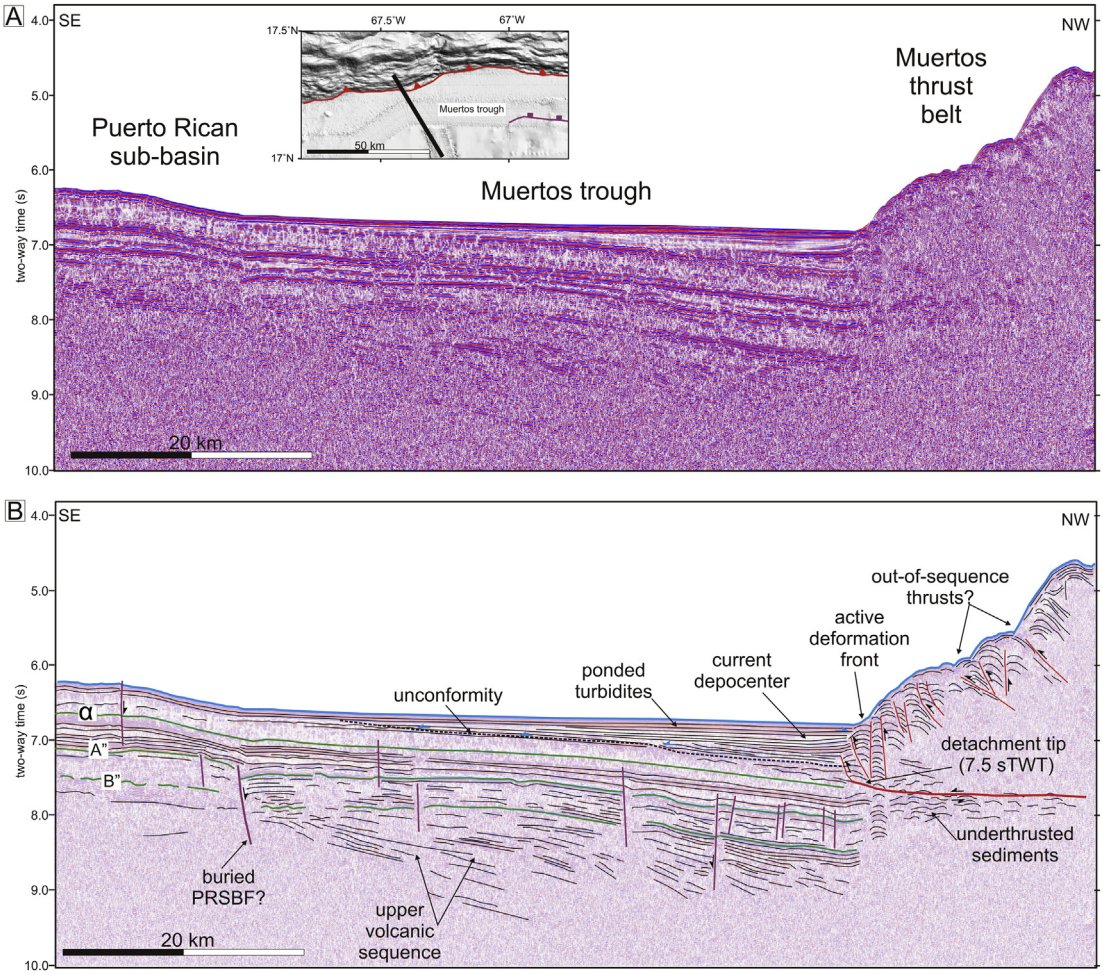

Figure 6. **A**) Stacked MCS profile. See location in the inset map. V.E. is 8.3× on the seafloor. **B)** Line drawing interpretation. See Figure 4B for legend. PRSBF = Puerto Rican sub-basin fault.

2014). In our study area, we have not identified any overthrusted basement high or igneous mound but they cannot be ruled out, because together with the along-strike changing structure of the incoming plate (c.f., Figs. 6 and 12), they could be responsible for the sinuous morphology of the deformation front. As an example, in our study area there is a 50 km-long salient (Ss in Fig. 3) that moves the deformation front ≈8 km southward of the theoretical normal position. We interpret the formation of this salient as a possible result of a deeper detachment in this zone (detachment tip at 8 sTWT in Fig. 5) relative to other localities along the deformation front where there is no salient (detachment tip at 7.3–7.5 sTWT in Figs. 6 and 12).

4.2. The Muertos margin province

The Muertos margin province forms the ≈700 km-long southern insular slope of the eastern Greater Antilles, from eastern Hispaniola to Puerto Rico (Fig. 1). In the south of Puerto Rico island, the Muertos margin province shows two distinct slope sub-provinces separated by a major along-strike concave slope break (thick black dashed line in Fig. 3; Figs. 4A and B): the Muertos thrust belt and the shelf slope (Fig. 2A). These two slope sub-provinces show significant differences along and across strike in the seafloor morphology, shallower structure and sedimentary processes. In addition, in the Muertos thrust belt two thrust systems can be distinguished, separated by a major along-strike convex slope break (thick yellow dashed line in Fig. 3; Fig. 4A and B): the lower thrust belt and the upper thrust belt (Figs. 2A, 4A and B).

4.2.1. The Muertos thrust belt

The Muertos thrust belt or fold-and-thrust belt sub-province is an E–W-trending S-verging imbricate system formed by the overthrusting and accretion of pelagic and turbiditic sediments against the island arc, defining a wedge of highly-deformed sediments (e.g., Ladd et al., 1981; Granja Bruña et al., 2014). The backstop of the accretionary system is formed by the shelf slope sub-province built presumably of igneous rocks from the inactive volcanic island arc (Griscom and Geddes, 1966; Jany, 1989; Granja Bruña et al., 2009). The growth of the accretionary system has adapted to the irregular morphology and position of the backstop, resulting in a significant along-strike asymmetry of the thrust belt (Fig. 2A). The thrust belt is ≈ 50 km-wide to the south of the Mona passage and it becomes progressively narrower eastward. Locally, to the south of the Jaguey spur (Fig. 2A), the backstop is located more southwards and the width of the thrust belt is drastically reduced from 45 km to 20 km. At 65.5°W the width of the thrust belt has decreased to <5 km, but there is still a narrow and continuous compressive active belt eastward along the toe of the insular slope of the St. Croix rise (SCR in Fig. 3). Here, the St. Croix rise acts as the backstop for this narrow deformed belt that extends eastward outside of the study area, but it is probably insignificant to the south of St. Croix Island.

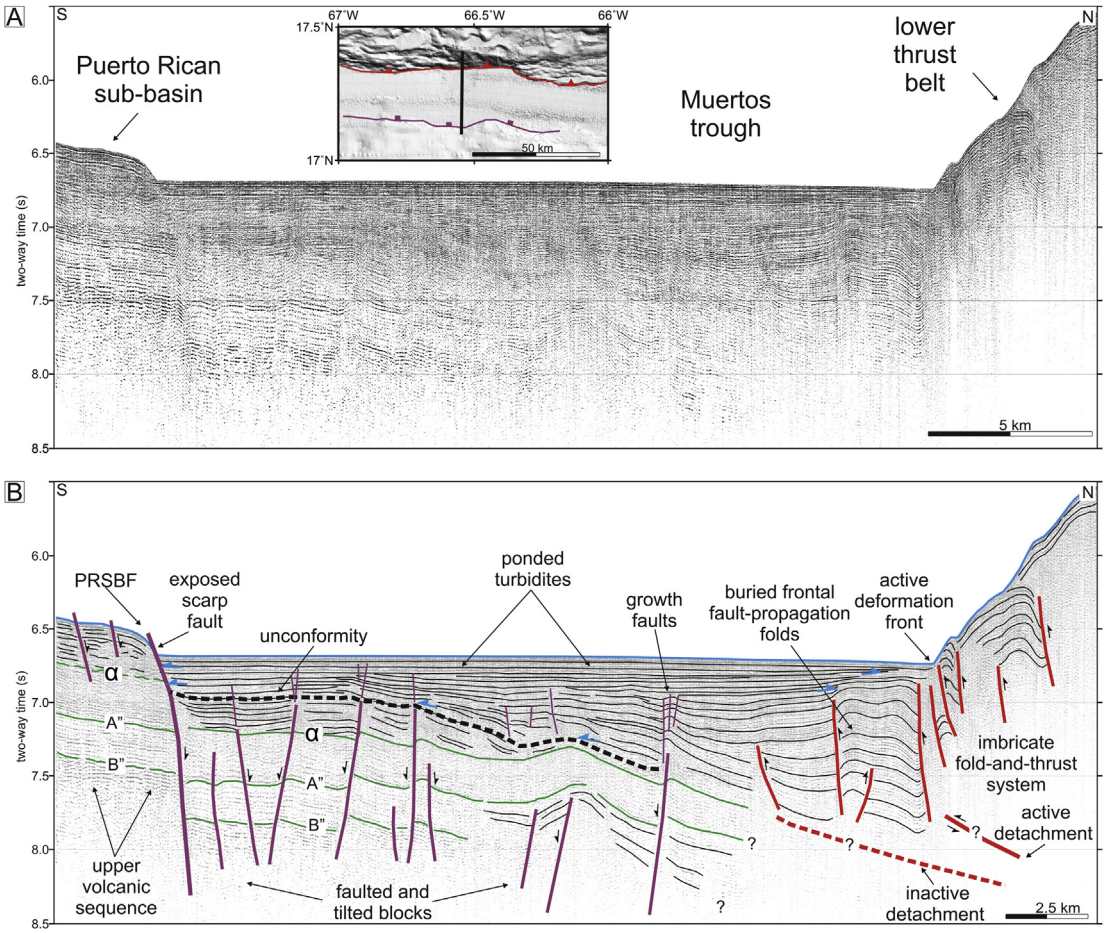

Figure 7. A) Post-stack migrated MCS profile. See location in the inset map. V.E. is 6.0× on the seafloor. **B)** Line drawing interpretation. See Figure 4B for legend. PRSBF = Puerto Rican sub-basin fault.

The surface expression of the imbricate thrust system consists of a succession of sinuous E–W-trending S-verging sub-parallel anticline ridges (Fig. 3). Anticline ridges are cored by thrust faults (i.e., fault-propagation folds; Figs. 5, 8 and 10) formed as a direct consequence of the accommodation of the convergence and the accretion of sediments. Although these thrust faults generally do not intersect the seafloor because of active sedimentation (i.e., blind thrusts), the associated anticline ridges mainly verging southwards make it possible to infer the existence and extent of N-dipping faults. The length of individual thrust faults varies between 5 and 30 km, and they can rarely be traced for more than 50 km along the strike (Fig. 3). The thrust faults are replaced along strike by other thrust faults forming an anastomosing structure in map view typical of imbricate thrust systems (c.f., McClay, 1992; Calassou et al., 1993). Between successive anticline ridges, there are elongated perched basins of variable size (i.e., piggy-back basins) frequently showing fanning, wedge-shaped growth packages of sediment occasionally buried by horizontal sediment sequences (Figs. 13 and 14). This fact implies that most basins and terraces show a complex depositional history, evidencing intermittent pulses of fault activity during the growth of the imbricate system as well as periods of quiescence (e.g., Smith et al., 2012). For instance, anticline ridges showing significant bathymetric expression bounding perched basins with recent tilted sequences are associated to thrust faults having recent activity (X in Fig. 13). Conversely, anticline ridges with small or absent bathymetric expressions bounding perched basins with horizontal parallel sediment beds suggest a lack of recent activity and/or smaller displacements in the associated faults (Y in Fig. 13).

Although the size, frequency and activity of the thrust faults is variable depending on the location across the imbricate system, there is a general pattern in the morphostructure that suggests that the activity of the faults in the Muertos thrust belt is more concentrated in the frontal region. This distribution of activity is known from other thrust belts (Moore and Karig, 1976), and was simulated by analogue and numerical modeling of imbricate thrust belts (e.g., Davis et al., 1983; von Huene and Scholl, 1991; Gutscher et al., 1996; Willett et al., 1993; Fuller et al., 2006). Notably, there appears to be a change in the size, frequency and activity of the thrusts evidenced by a broad along-strike convex slope break, which marks an intra-thrust belt boundary separating the lower and upper thrust belts (thick yellow dashed line in Fig. 3; Fig. 4A). The existence of intra-thrust belt boundaries has been interpreted as a result of the reactivation of arcward thrusts and/or formation of out-of-sequence thrusts resulting in a more complex distribution of deformation (e.g., Hardy et al., 1998; Lohrmann et al., 2003; Park et al., 2002; Kopp and Kukowski, 2003). The convex slope break that marks an intra-thrust belt boundary in the Muertos thrust belt is associated with longer and broader anticlines ridges that are presumably cored by larger active thrust faults. However, the limited penetration of seismic data prevents the identification of these faults as reactivated arcward thrusts and/or neoformed out-of-sequence thrusts (Figs. 4B and 13).

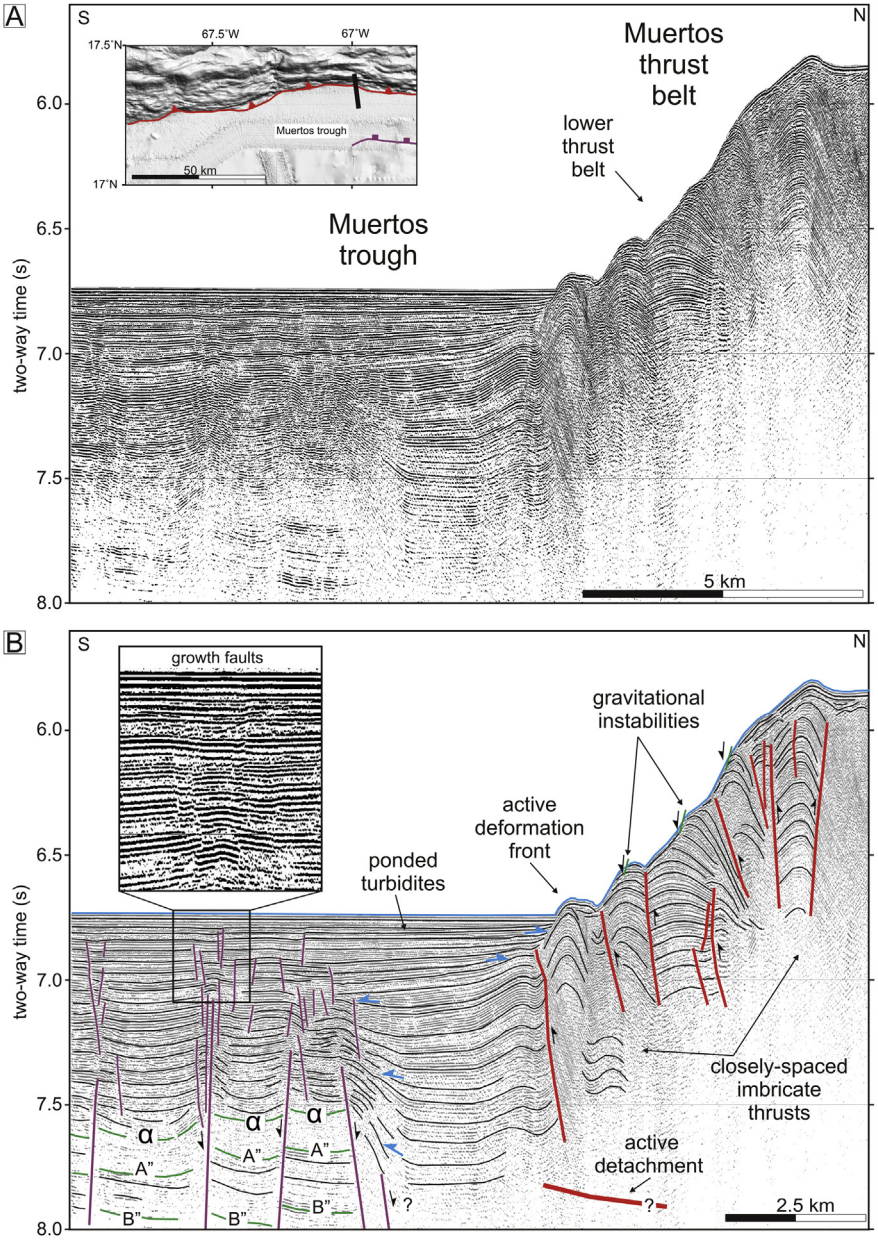

Figure 8. A) Post-stack migrated MCS profile. See location in the inset map. V.E. is 6.0× on the seafloor. **B)** Line drawing interpretation. See Figure 4B for legend.

4.2.1.1. Lower thrust belt. The lower thrust belt occupies a continuous band of steep and stepped slope between the deformation front and the convex slope-break (Fig. 2A). This thrust belt extends continuously along the base of the slope and continues eastward along the base of the slope of the St. Croix rise (Fig. 3). The regional slope varies between 7° and 10° (App. C) and shows local gradients of ≈20° associated to individual anticline ridges with evidence of gravitational instabilities (Figs. 8 and 10). The surface expression of the lower thrust belt is a succession of closely-spaced small anticline ridges suggesting that the active deformation is distributed in many small thrust faults (Figs. 8 and 12). The anticline ridges are covered by a thin blanket of growth sediments related to fault activity and the growth of the ridge. The inter-ridge space is occasionally occupied by small elongated piggy-back basins (Fig. 10).

4.2.1.2. Upper thrust belt. The upper thrust belt occupies a continuous band of stepped slope, forming a mid-slope terrace with variable extension along-strike between the convex and concave slope breaks (Figs. 2A, 4A and B). Contrary to the lower thrust belt that extends continuously eastwards along the base of St. Croix rise, the upper thrust belt disappears east of 66°W (Fig. 3). Except in a few isolated broad anticline ridges, the mid-slope terrace has gentler slopes (1°–3°) showing smoother seafloor morphology (App. C). The gentler seafloor gradients, together with the existence of occasional E–W-trending anticline ridges that act as topographic barriers trapping the turbiditic sedimentary supplies from upslope regions, contribute to the increased sediment accumulation, yielding larger perched basins and terraces. As a result, most of the imbricate structures are buried by thick slope sediments blurring the seafloor expression of the anticline ridges (Fig. 13). Many terraces are located along the base of the shelf slope sub-province and are connected with the mouths of numerous canyons (Fig. 3). These perched basins can extend for over 25 km along strike and contain up to 2 sTWT (~2 km) of sediment thickness (Fig. 14). The active

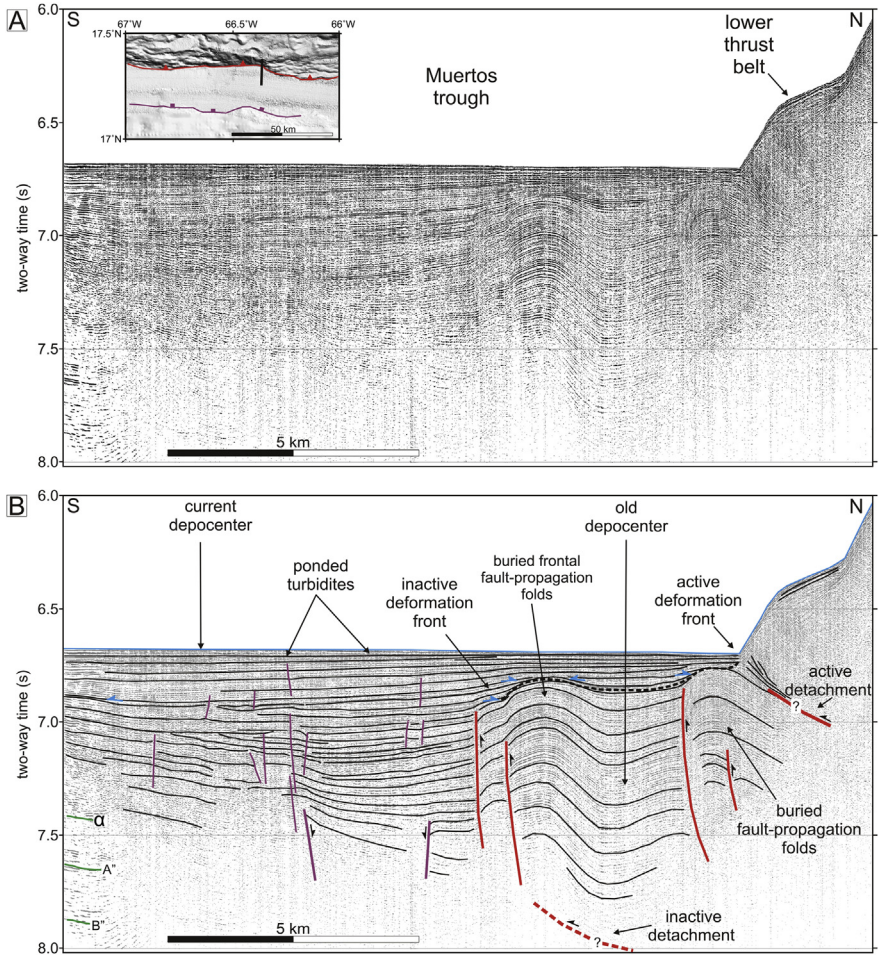

Figure 9. A) Post-stack migrated MCS profile. See location in the inset map. V.E. is 6.0× on the seafloor. **B)** Line drawing interpretation. See Figure 4B for legend.

deformation in the upper thrust belt seems to be mainly concentrated in local thrust faults with larger dip-slip displacements, forming longer and higher anticline ridges that are frequently associated with recent tilted sequences in the adjoining basins (Fig. 14). The progressive thickening of the slope sediment deposits, together with the vertical growth of the underlying thrust belt, contributes locally to yield broad antiforms and the inversion of perched basins (Fig. 14). These processes are occasionally accompanied by the existence of frequent gravity-driven accommodation faults in the anticline hinge zone (i.e., bending-moment normal faults), driving a partial collapse of the ridge flanks. Accommodation faults are frequent in the mid-slope terrace and they are favoring downslope creep processes and S-directed gravity flows (Fig. 3). The existence of extensional tectonics in the rear zones of accretionary systems is widely documented from sand-box analogue modeling as a mechanism of balancing the taper angle (e.g., Davis et al., 1983).

4.2.2. The shelf slope

The shelf slope sub-province extends from the edge of the insular platform to the concave slope break (Figs. 2A, 4A and B). This province is probably cored by the rocks of the inactive island arc (Griscom and Geddes, 1966; Jany, 1989; Granja Bruña et al., 2009) covered by a thick package of layered slope sediments (Fig. 4B). The average gradients are between 4° and 9°, and occasionally >16° associated with structural steps and highly-incised canyons (App. C). There are many observations for active gravitational processes (i.e., downslope creep) and slope failures over all of the province, but they are more intense in the western region at the Jaguey spur where the shelf slope province is wider (Fig. 3). The main geomorphic features are a dense network of relatively straight channel-canyon systems and gullies flowing from the edge of the insular shelf. Most of the gullies do not appear to cut the edge of the insular shelf except at the active Guayanilla channel-canyon system (Fig. 2A). This system shows at least six deep erosive channel-canyon systems connected with onshore rivers that have yielded headward erosion almost to the shoreline, reducing dramatically the extension of the insular shelf (Fig. 3). In general, there is a tendency for smaller canyons and slope gullies to coalesce downslope, forming bigger channel-canyons systems that debouch in the mid-slope terrace (i.e., upper thrust belt) and lose their surface expression. There are no observable fan-shape deposits emanating from the mouth of the bigger feeder channel-canyons systems. The absence of fans at the mouth of these systems could be a consequence of strong axial bottom currents in the channel-canyons systems (Underwood and Moore, 1995) or, more likely, low rates of sediment supply and transport. Swath bathymetry data do not show any distinctive canyon-channel systems bypassing the E–W-trending anticline ridges of the mid-slope terrace. Therefore, the transported sediment along the channel-canyon systems is mainly deposited along the mid-slope terrace, forming relatively thick slope deposits and perched basins. This sediment accumulation helps bury partially the anticline ridges in the mid-slope terrace. The GLORIA mosaic shows that the sandy

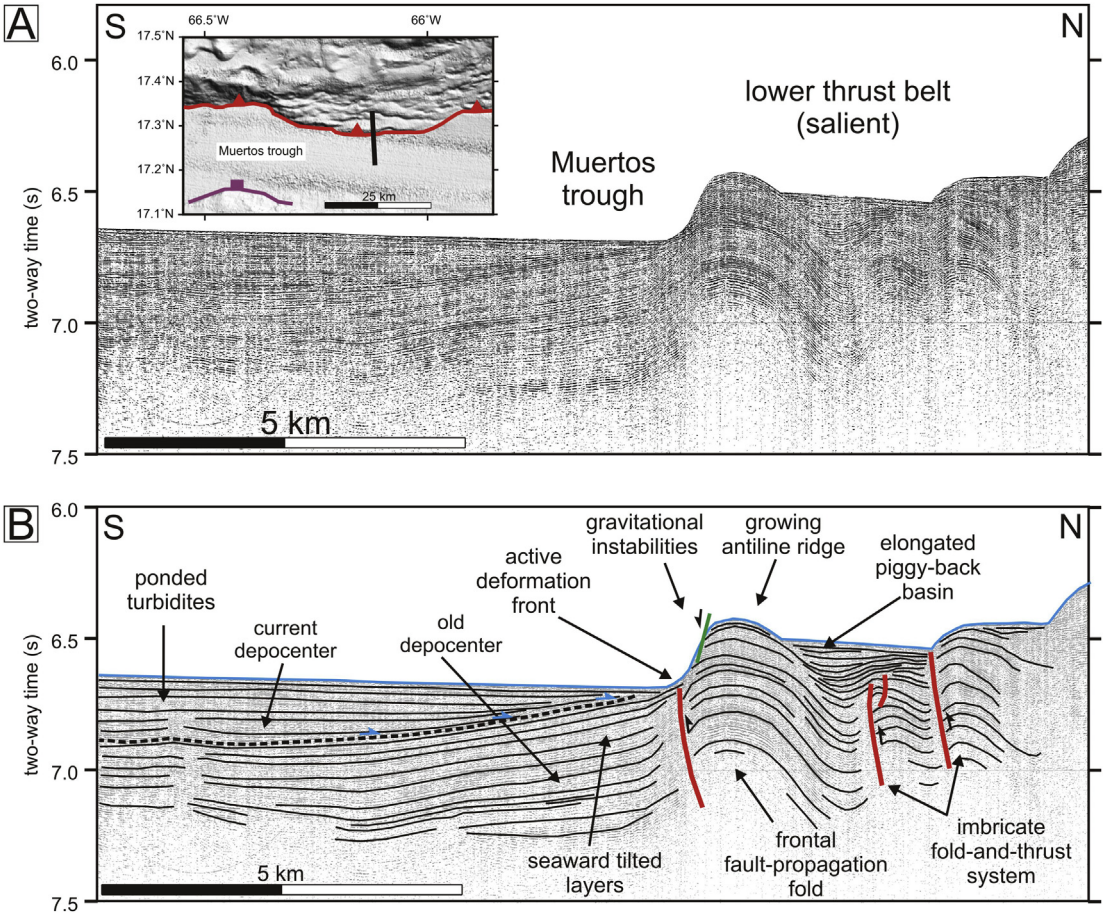

Figure 10. **A**) Post-stack migrated MCS profile. See location in the inset map. V.E. is 6.0× on the seafloor. **B)** Line drawing interpretation. See Figure 4B for legend.

turbidite sediments, which are characterized by high backscatter (Masson and Scanlon, 1991; App. D), are dispersed downward over the mid-slope terrace and occupy locally the troughs between thrust slices.

4.2.2.1. Investigator fault zone. The Investigator fault zone consists of an E–W-trending 130 km-long band of active extensional deformation located along the shelf slope province in the upper southern slope of Puerto Rico island (IFZ in Fig. 2A). This fault zone is characterized by a major branch fault surrounded by numerous minor faulting. The major branch fault shows differential surface expression along strike and has three distinct sectors offset by relay ramps (RR in Fig. 3) that reflect significant changes in the magnitude and distribution of the deformation: western sector, central sector and eastern sector.

4.2.2.1.1. Eastern sector. In the eastern sector (EIFZ in Fig. 3), the most significant feature is a ~080°-trending 45 km-long deep valley which is flanked southward by the outstanding Investigator ridge (Figs. 2A and 15). This deep valley was explored by Case and Holcombe (1980) and registered as the "Investigator canyon" in the International Hydrographic Organization (www.iho.int). From the viewpoint of the geomorphology, the expression "canyon" is generally used to refer to a deep, steep-sided valley with an axial slope of 4.5° (Allaby, 2008). This trough is deep and steep-sided but has axial slopes of <1.7°. We therefore propose more appropriately to refer to this feature as the "Investigator valley". This valley disconnects the shorter drainage network developed in the upper zone of the sub-province from the longer canyons flowing along the lower zone of the slope that finally debouch in the mid-slope terrace (Fig. 3). The axial zone of the valley is occupied by sediments forming an elongated basin with a gentle westward axial slope. This gentle slope favors a westward through-going sediment conduit that collects the turbiditic sedimentary supplies from the upward slope (App. D). The Investigator ridge has steep sides (>16°) and reaches a height of 750 m over the Investigator valley seafloor but it loses height along strike (Figs. 3 and 15C). The Investigator ridge consists of a faulted bathymetric high whose north flank is the exposed scarp of a normal fault that is the main branch of the Investigator fault (Fig. 15A–C). Deeper fanning sediment beds inferred in the elongated basin formed in the bottom of the valley and the uniformly S-dipping sediments covering the Investigator ridge suggests certain amount of southward tilting (Fig. 15A and C). This southward tilting process seems not to be active since recent sediments are horizontally ponded along the fault trace (Fig. 15A–C). However, N–S-trending extension seems to be recent because of the existence of mini-fault scarps deforming the basin seafloor (Fig. 15B). The southern flank of the Investigator ridge is characterized by a network of relatively straight gullies that preferentially start at the summit of the Investigator ridge and reach the mid-slope terrace. The slope of the southern flank averages 6°–9° and occasionally shows several along-strike NNE–SSW-trending steps (Fig. 3). These steps are caused by minor faults that yield frequent slope failures and disrupt the gullies (dashed purple lines in Fig. 3). The Grappler ridge is a SE-tilted block that extends eastward connecting with the Grappler bank (Figs. 2A and 15A). The Investigator fault ends where it is cross-cut by the NE–SW-

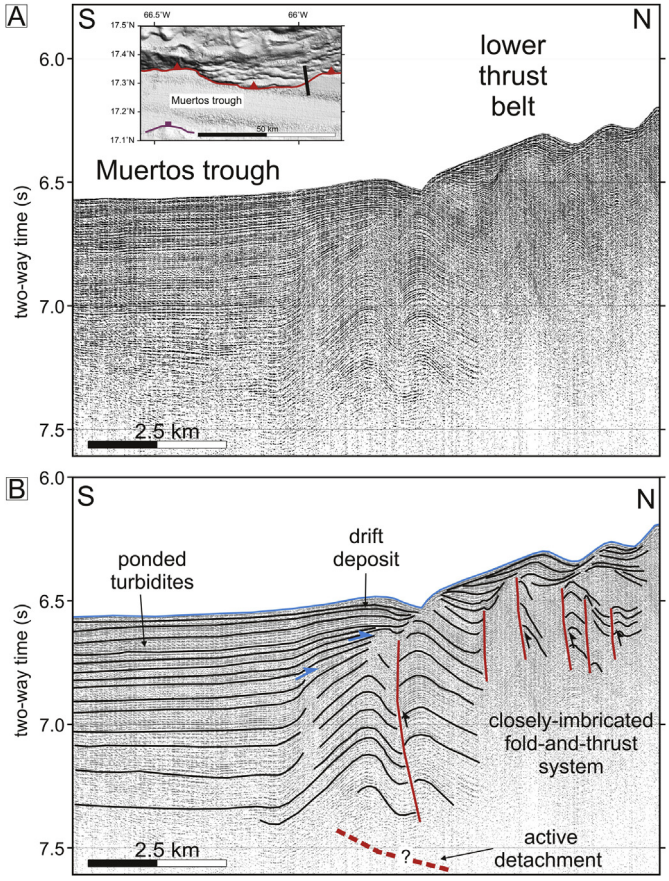

Figure 11. A) Post-stack migrated MCS profile. See location in the inset map. V.E. is 6.6× on the seafloor. **B)** Line drawing interpretation. See Figure 4B for legend.

trending Grappler ridge. The Investigator valley can be continuously observed eastward until it merges with the small benched Grappler sub-basin via a narrow saddle (≈1600 mbsl; Fig. 2A). The thickness of the sediments accumulated along the Investigator valley varies from 0.3 sTWT in the western zone (Fig. 15A) to >0.7 sTWT where the trough connects the small benched Grappler sub-basin (Fig. 15C). The Grappler sub-basin is flanked in the southeast by the Grappler ridge and bank and shows frequent evidence of active NW–SE-oriented extension and southward tilting (Fig. 15A).

4.2.2.1.2. Central sector. The morphology of the Central sector (CIFZ in Fig. 3) is dominated by numerous straight high-incised gullies and a 085°–090°-trending bench (Fig. 2A; App. C). This bench is a 30 km-long feature, which evolves progressively along strike from a bench-like feature in the east, to a smooth convex slope break broken by minor fault-steps in the west (Fig. 16). The bench is the result of the activity of a major N-dipping normal fault that has yielded a southward block rotation (Fig. 16A–C). The dip-slip displacement on this major fault decreases progressively westward and is eventually replaced by numerous small faults that form a convex slope break along the shelf slope. In the east the deformation is concentrated in a main fault, while in the west it is distributed in numerous small faults, resulting in the evolution from the benched morphology to the convex slope break (Fig. 16). In the eastern zone the bench is wider and forms an elongated trough that collects turbiditic supplies from the upward slope without a defined axial slope. Occasionally, the sediments completely fill the trough, reaching a thickness of at least 0.3 sTWT and yielding the bench-shaped feature (Fig. 16A). Recent sediments are ponded, partially filling the trough and forming an elongated perched basin. However, there are buried sequences of fanning beds which record a more intense stage of dip-slip motion of the fault (Fig. 16A). The bigger gullies cross the bench without interference by the slope break, continue southward along the lower slope and debouch in the mid-slope terrace where they lose their surface expression (e.g., Guayanilla canyon system; Fig. 3). Upslope and downslope from the bench and the convex slope break, the shelf slope province is occupied by a thick cover (locally >1 sTWT) of layered sediments that are frequently affected by minor faulting and associated slope failures and gravity instabilities.

4.2.2.1.3. Western sector. The geomorphic expression of the western sector (WIFZ in Fig. 3) is completely different from that of the central and eastern sectors where the major faults form prominent valleys, benches or convex slope breaks. In the western sector the deformation seems to be distributed on many faults that deform the seafloor over a wide band. This distribution of the deformation has formed a NE–SW-trending bathymetric high separated from the shelf slope (Jaguey spur; Fig. 2A). The Jaguey spur is covered by a sedimentary sequence at least 0.6 sTWT thick and shows recent moderate deformation (Fig. 17). The sediment beds show minor growth faulting, together with wide antiforms and synforms that deform the seafloor. This hummocky surface is devoid of erosional drainage features because this structurally-controlled high forms a salient in the shelf slope sub-province that diverts the paths of the canyons and gullies to the west. The significant sediment accumulation on the top of a bathymetric high (inverted basin? in Fig. 17B), which is isolated from any channelized supply, probably arises from the uplift of the underlying rocks of the Jaguey spur. The existence of a thick sedimentary sequence and recent deformational features on the top of the Jaguey spur suggests that uplift could be presently active. The gravity and geomagnetic anomalies at the Jaguey spur suggest that the basement of the spur is made of igneous rocks (Griscom and Geddes, 1966; Jany, 1989; Granja Bruña et al., 2010). In the upper southern flank the bounding fault forms a large bathymetric scarp where the basement may outcrop, but there are no dredge samples from this zone. The northern and particularly the southern steep flanks that define the Jaguey spur (as much as 20°), together with the recent deformation, suggest that they are particularly prone to gravity failure, downslope creep and re-sedimentation by large-scale mass movements. These steep gradients are mainly caused by two large dip-slip normal faults bounding the Jaguey spur (Fig. 17). The topography of the Jaguey spur decreases westward and it is buried beneath the thick slope sediments of the perched basins developed in the upper thrust belt. The western termination of the Investigator fault zone takes place in the Jaguey spur region. West of the Jaguey spur, the shelf slope sub-province is reestablished again as part of the Mona passage extensional tectonics (Fig. 3; Grindlay et al., 2005b; Chaytor and ten Brink, 2010).

4.3. The insular shelf province

The insular shelf province is formed by the Puerto Rico–Virgin Island carbonate platform with a sinuous seaward edge that extends along the south coast of Puerto Rico (Fig. 2A; Trias, 1991; van Gestel et al., 1998; Mann et al., 2005). The shelf edge, with water depths of 10–45 m, is characterized by early Pleistocene drowned prominent-edge reefs (Garrison, 1969; Beach and Trumbull, 1981) and the shelf width varies between almost zero, as in the Guayanilla channel-canyon system, to a maximum of 16 km eastward of Caja de Muertos island (Fig. 2A). The sinuous edge of the platform forming numerous scalloped embayments is a result of the progressive escarpment erosion yielded by the channel-canyon systems and slope mass failures (c.f., Mullins and Hine, 1989). The

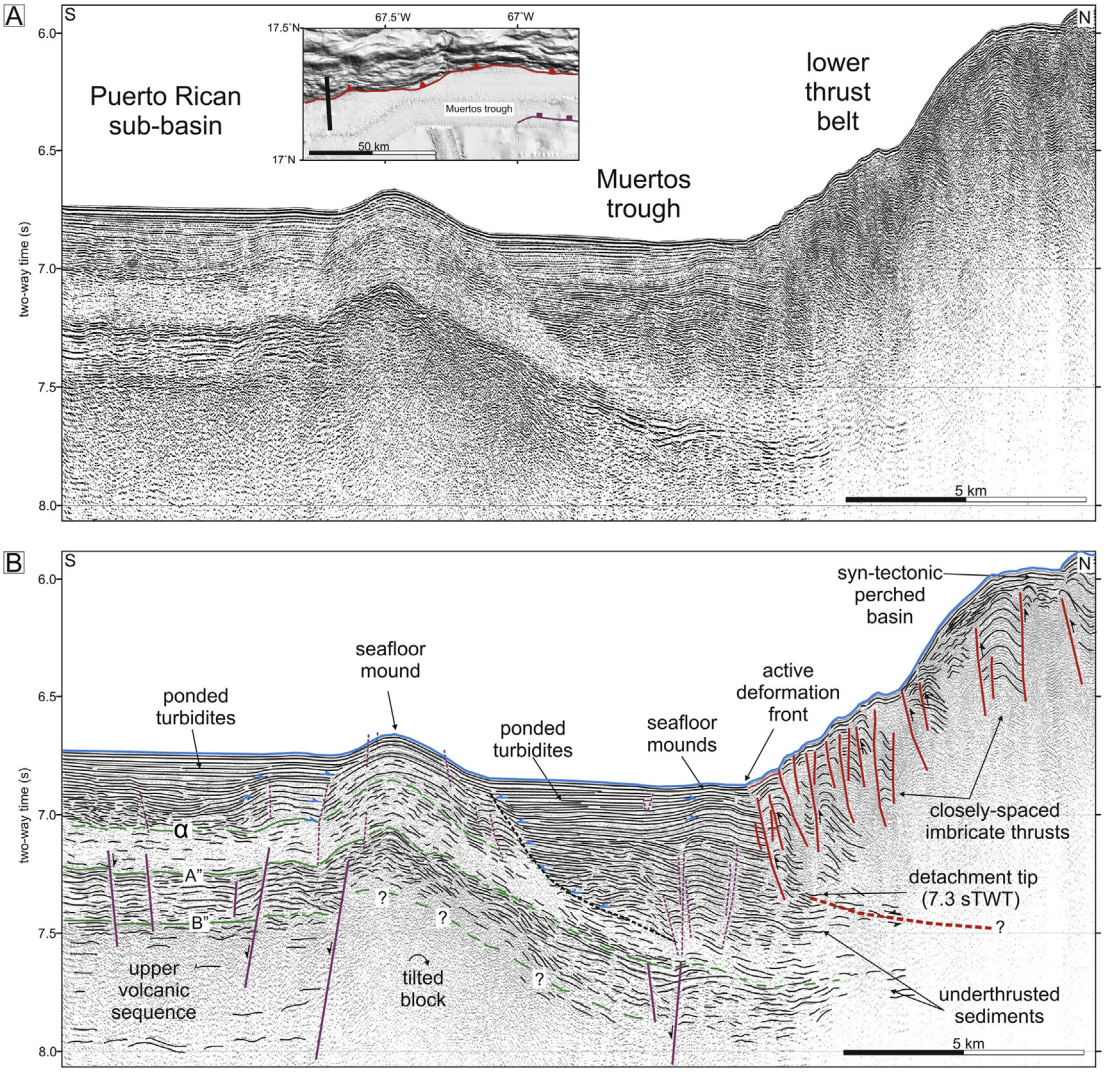

Figure 12. A) Post-stack migrated MCS profile. See location in the inset map. V.E. is 4.9x on the seafloor. **B)** Line drawing interpretation. See Figure 4B for legend.

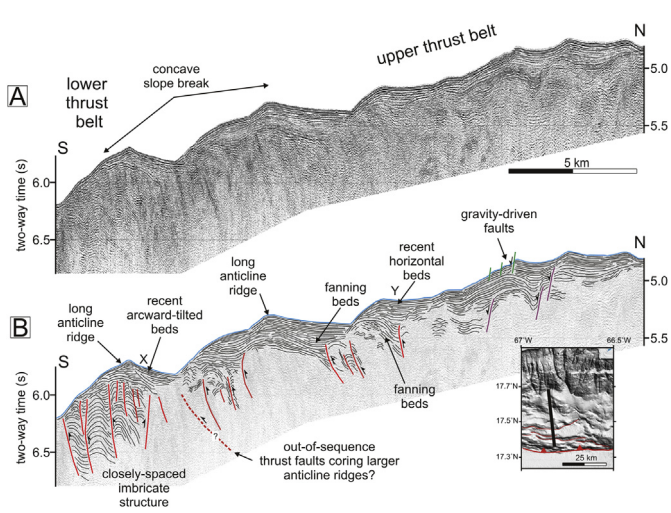

Figure 13. A) Post-stack migrated MCS profile. See location in the inset map. V.E. is 6.0× on the seafloor. **B)** Line drawing interpretation. See Figure 4B for legend. X and Y are locations referred to in Section 4.2.1 (active and inactive piggy-back basins respectively).

largest embayment is 37 km across by 8 km wide and encompasses the head of the Guayanilla channel-canyon system.

The structure of the insular shelf to the south of Puerto Rico was studied using seismic reflection data (Fig. 2B; Denning, 1955; Garrison, 1969; Glover, 1971; Case and Holcombe, 1980; Beach and Trumbull, 1981; van Gestel et al., 1998; Mann et al., 2005). However, the structure is not fully understood because of the poor penetration of these reflection profiles through the shallow hard carbonate grounds. The insular shelf province is dominated by an extensional tectonics with two fault trends affecting the uppermost part of the sedimentary section (Fig. 3; Mann et al., 2005): NE–SW- and E–W-oriented faults. Most faults are NE–SW-trending and have caused an alternation of structurally-controlled highs and lows on the seafloor, some of which have onshore continuity (e.g., Bajo Tasmanian fault; BTF in Fig. 3). Some faults show significant throw near the shelf edge, such as the Caja de Muertos fault with 1.1 Km (CMF in Fig. 3), but this throw disappears where the fault crosses the shoreline. In contrast, Holocene ruptures and recent uplift of beach ridges where some faults cross the shoreline suggest that faults may have recent activity (Bajo Tasmanian fault and Ponce fault; BTF and PF in Fig. 3; Garrison, 1969; Mann et al., 2005). The Central fault (CF in Fig. 3) is an E–W-trending fault that consists

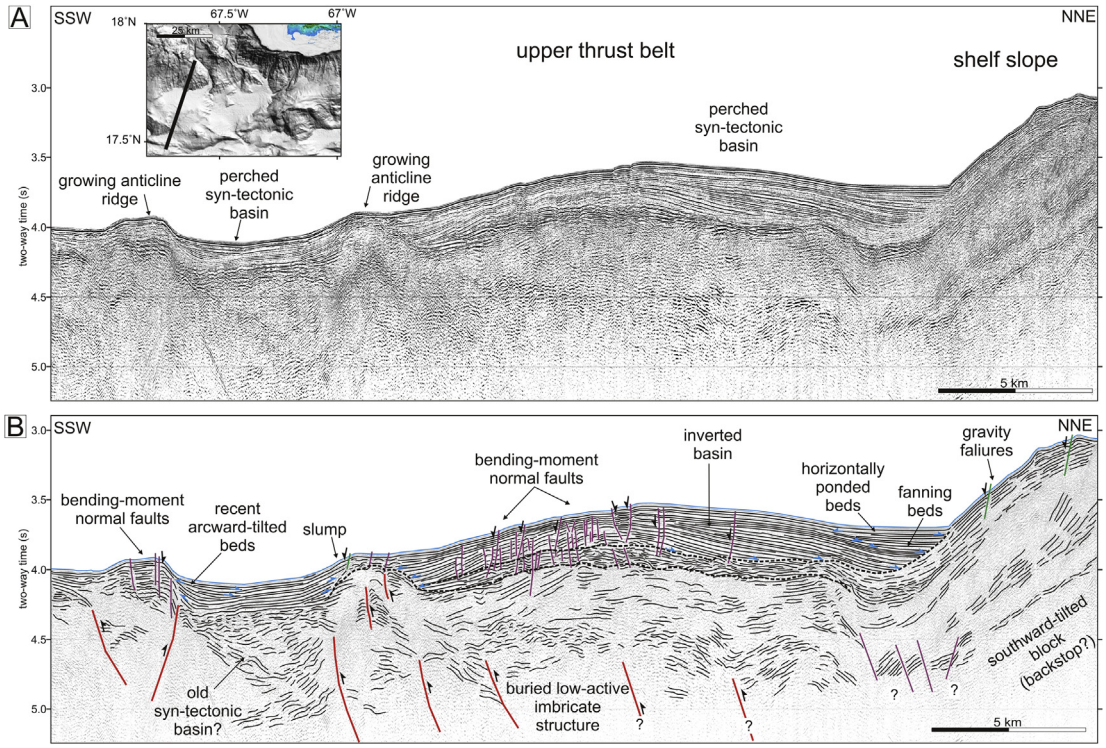

Figure 14. **A**) Post-stack migrated MCS profile. See location in the inset map. V.E. is 4.9× on the seafloor. **B)** Line drawing interpretation. See Figure 4B for legend.

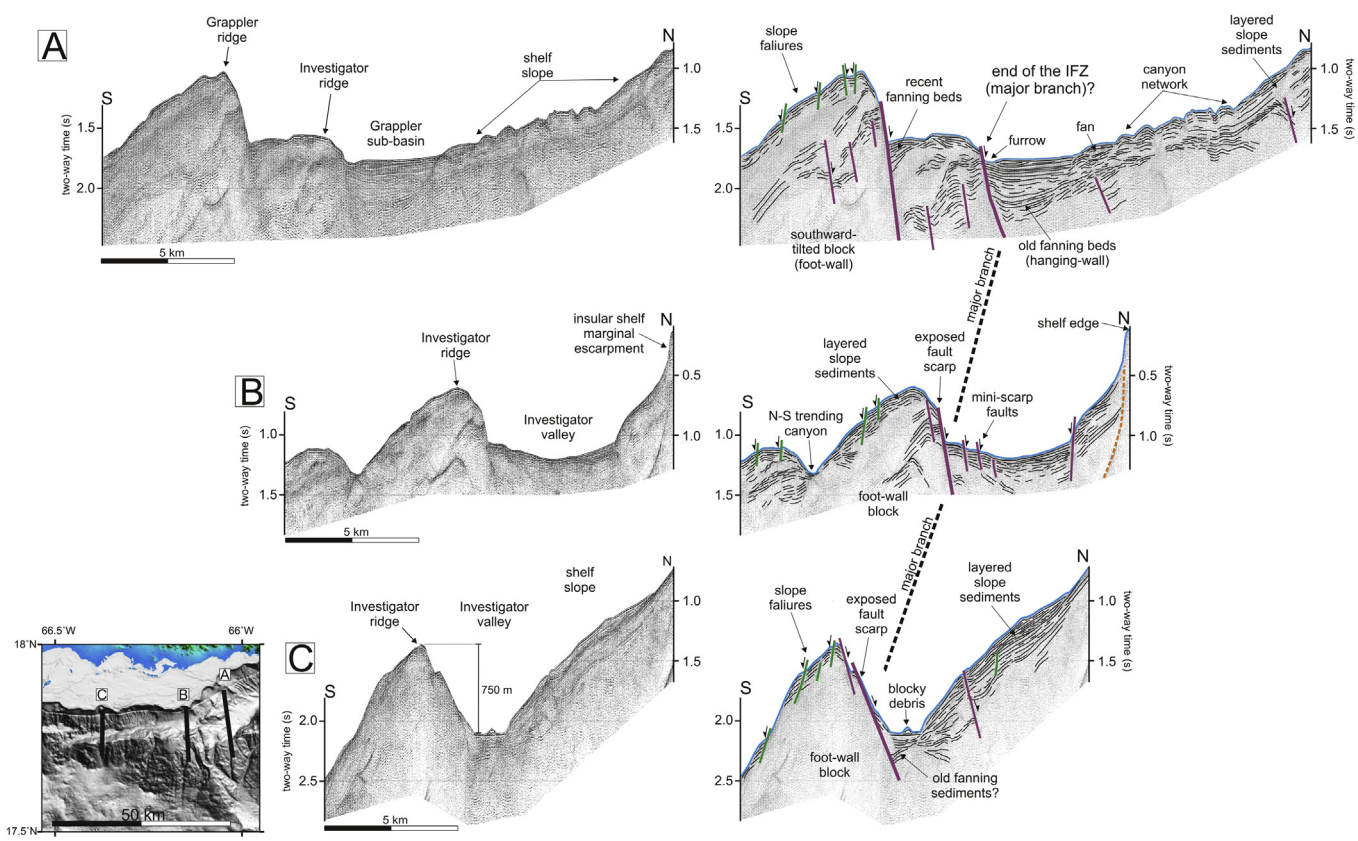

Figure 15. **A, B, C)** Post-stack migrated MCS profiles on the left and line drawing interpretation on the right. See location in the inset map. V.E. is 6.0× on the seafloor. See Figure 4B for legend. IFZ = Investigator fault zone.

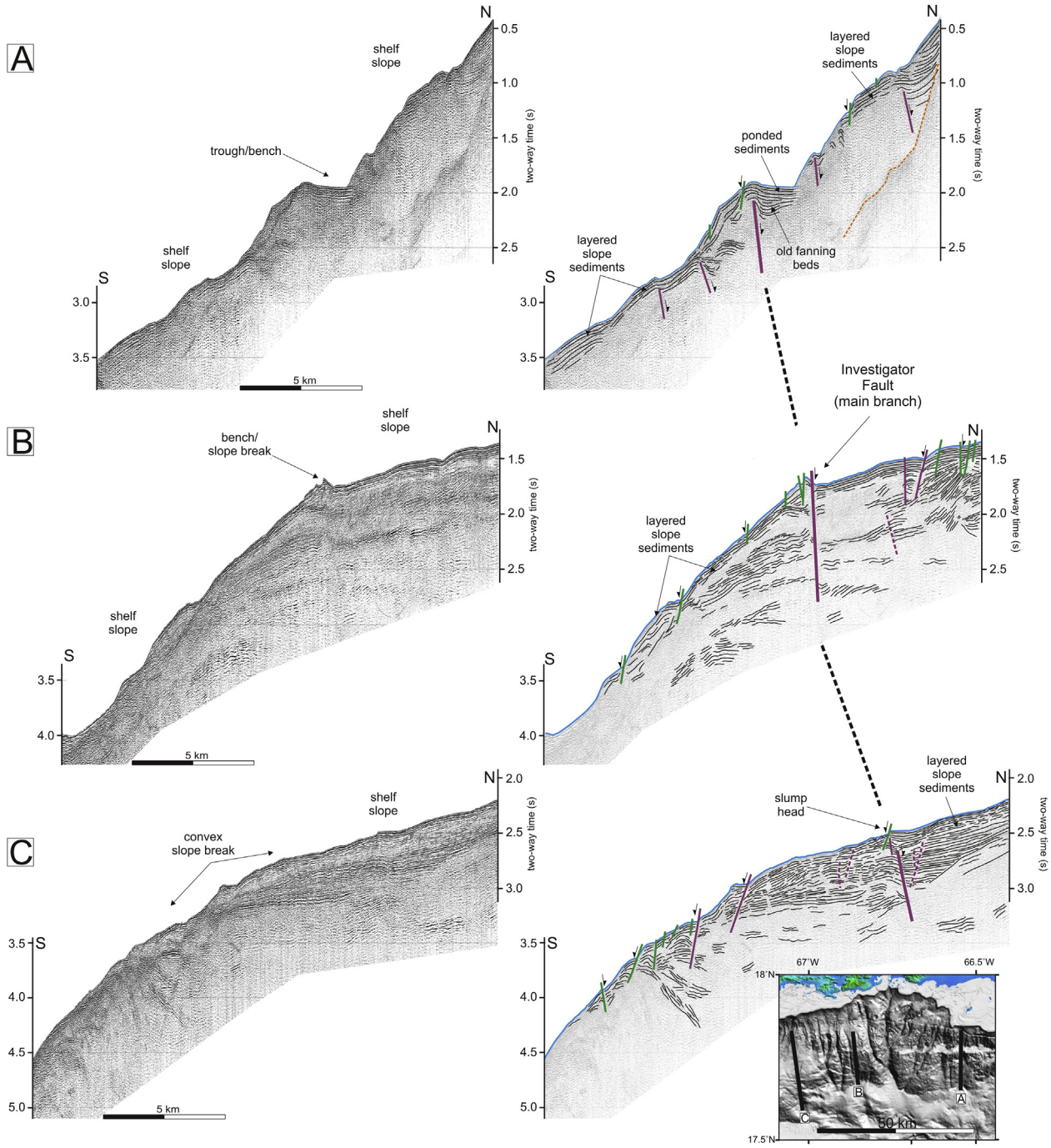

Figure 16. A, B, C) Post-stack migrated MCS profiles on the left and line drawing interpretation on the right. See location in the inset map. V.E. is 6.0× on the seafloor. See Figure 4B for legend.

of three individual N-dipping segments that reach the seafloor, suggesting recent activity (Figs. 16 and 17 in Mann et al., 2005).

4.4. Western Anegada passage province

The morphology of the western Anegada passage province (Fig. 2A) shows a succession of NE–SW- and E–W-trending deep basins and steep ridges indicating a complex structure. The main physiographic features are the Virgin Islands basin, the Vieques basin, the Whiting basin and ridge, the Grappler bank and ridge and the St. Croix rise (Fig. 2A and 18). The structure of the Anegada passage is not yet fully understood because of the superposition of several tectonic stages (Mann et al., 2005). We focus our study on the description of the westernmost zone of the passage, including the Whiting basin and ridge, the western Virgin Islands basin and the western St. Croix rise. The present study has to be complemented with the interpretation provided over a more extended region of the Anegada passage (e.g., Jany et al., 1990; Raussen et al., 2013; Chaytor and ten Brink, 2014).

4.4.1. Whiting basin and bounding ridges

The Whiting basin is a rhomboidal-shaped depression in map view located off the southeast of Puerto Rico (Fig. 2A). This basin is separated from the coast of Puerto Rico and the Vieques islands by a

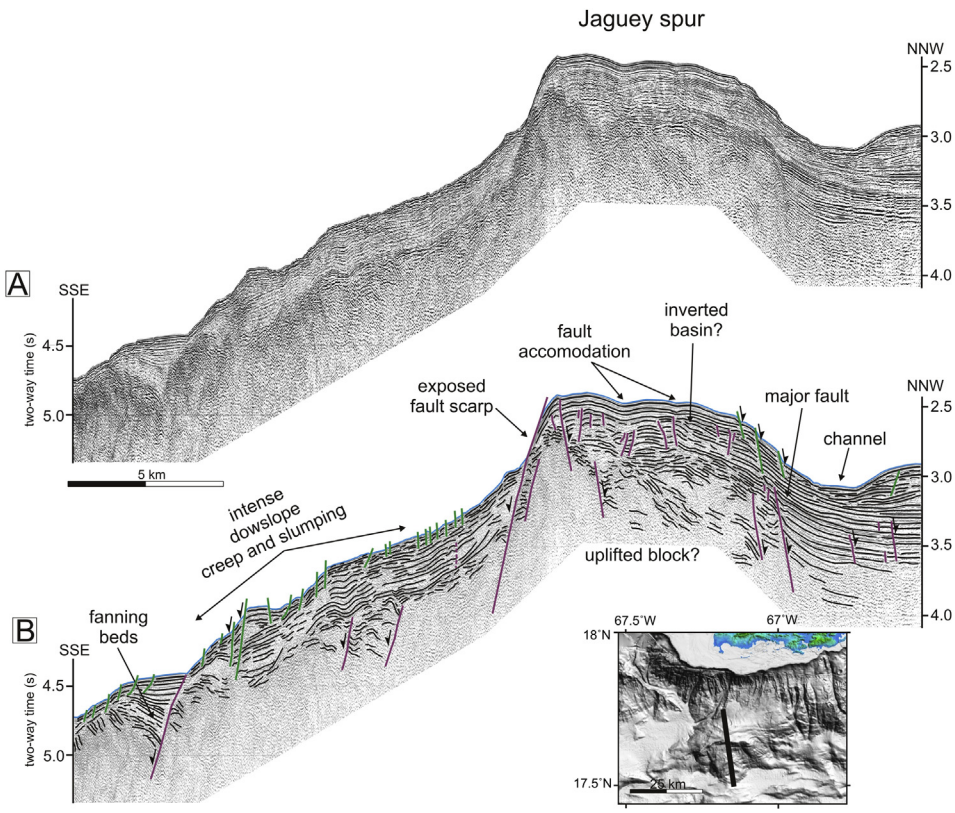

Figure 17. **A**) Post-stack migrated MCS profile. See location in the inset map. V.E. is 4.9× on the seafloor. **B)** Line drawing interpretation. See Figure 4B for legend.

narrow scalloped carbonate insular shelf. The floor of the basin covers an area of approximately 325 km^2 at depths between 1900 and 1990 m (App. A). The basin is bounded by steep walls (i.e., exposed fault escarpments) and bathymetric highs resulting in a confined NE–SW-trending depression. Seismic images evidence that the Whiting basin is formed on a half-graben structure filled by a sedimentary section of at least 1.5 sTWT of thickness (Figs. 19, 20 and 21). The basin infill shows fanning, wedge-shaped growth packages of sediment onlapping northwards previous sequences deposited on a S-tilted hanging-wall block. The recent sediments consist mainly of sand and silty-sands near the edges and clay-rich silts in the deeper zones of the basin interior (Chaytor and ten Brink, 2014). The accommodation space was created by the dip-slip displacement of NE- (Fig. 20) and NW-dipping (Figs. 19 and 21) faults that have yielded the large tilting of the hanging-wall blocks. Seismic images show a large dip-slip displacement on faults bounding the basin, but no strike-slip displacement can be inferred, as was also suggested by Jany et al. (1990). Most of the sedimentary sequences close to the faults are deformed by drag along the fault but this deformation is not always observed in the recent beds. Locally, in the southern edge of the basin, faults show evidence for recent tectonic activity as seen from the occasional seafloor rupturing (Fig. 19). However, at the north edge and in the interior of the basin, except where there are fan-shaped deposits, recent sediments are horizontal to sub-horizontal suggesting a low rate of recent deformation. On the other hand, the documented low rates of sediment accumulation (<1 mm/yr) suggest that the interior of the basin has been relatively quiet in recent times (Chaytor and ten Brink, 2014).

The basin is bounded to the northwest by a 10–15°-steep shelf slope which is highly-incised by canyons and gullies that debouch into the basin and form fan-shaped depositional systems and sediment wave fields along the northern bound of the basin (Figs. 3 and 19). Although the steep and irregular morphology of the seafloor produces noisy seismic images, this shelf slope seems to be controlled locally by recent faulting (Figs. 19 and 22) and in the northeastern zone associated with southward block tilting (Fig. 21). The basin is bounded in the southwest by a large 1900 m-high NE-facing escarpment (15°–70° of dip) showing locally slope failure features (Fig. 20; App. C). The orientation of this escarpment suggests that it could be the offshore extension of the Great Southern Puerto Rico fault zone (GSPRFZ in Fig. 3). The GSPRFZ was interpreted onshore as a NW–SE-trending left-lateral strike-slip fault that crosses the coastline in the southeast of Puerto Rico island and extends offshore southeastward. The surface expression of the fault on the insular shelf comprises a several hundred meter wide NW–SE-oriented band of deformation showing a succession of several fault scarps reaching ≈10 m in height. Glover (1971) and Erikson et al. (1990) documented that fault traces in the island shelf do not cut post-Eocene sediments. Mann et al. (2005) suggested the existence of Late Quaternary activity in the insular shelf based on poor quality SCS profiles, since the presence of carbonate hard grounds yields high-amplitude seafloor reflections with limited sub-seafloor penetration. In the shelf slope the fault trace can be outlined along a NW–SE-oriented canyon system that flows into the western Whiting basin (Fig. 21). However, the highly-irregular seafloor morphology yielded by the activity of the canyons (alternation of sedimentary ridges and troughs) produces noisy seismic images preventing the identification of the structure of the Great Southern Puerto Rico fault zone (Fig. 22). This fault continues southeastward to form a NE-facing scarp that separates the seafloors of the small benched Grappler sub basin and the Whiting basin (Figs. 3 and 22). The Grappler sub-basin shows a 0.5 sTWT-thick sequence of fanning beds deposited over a SE-tilted block and buried by 0.2 sTWT-thick drift deposits (Fig. 22). The fault continues southeastward forming the large NE-facing escarpment

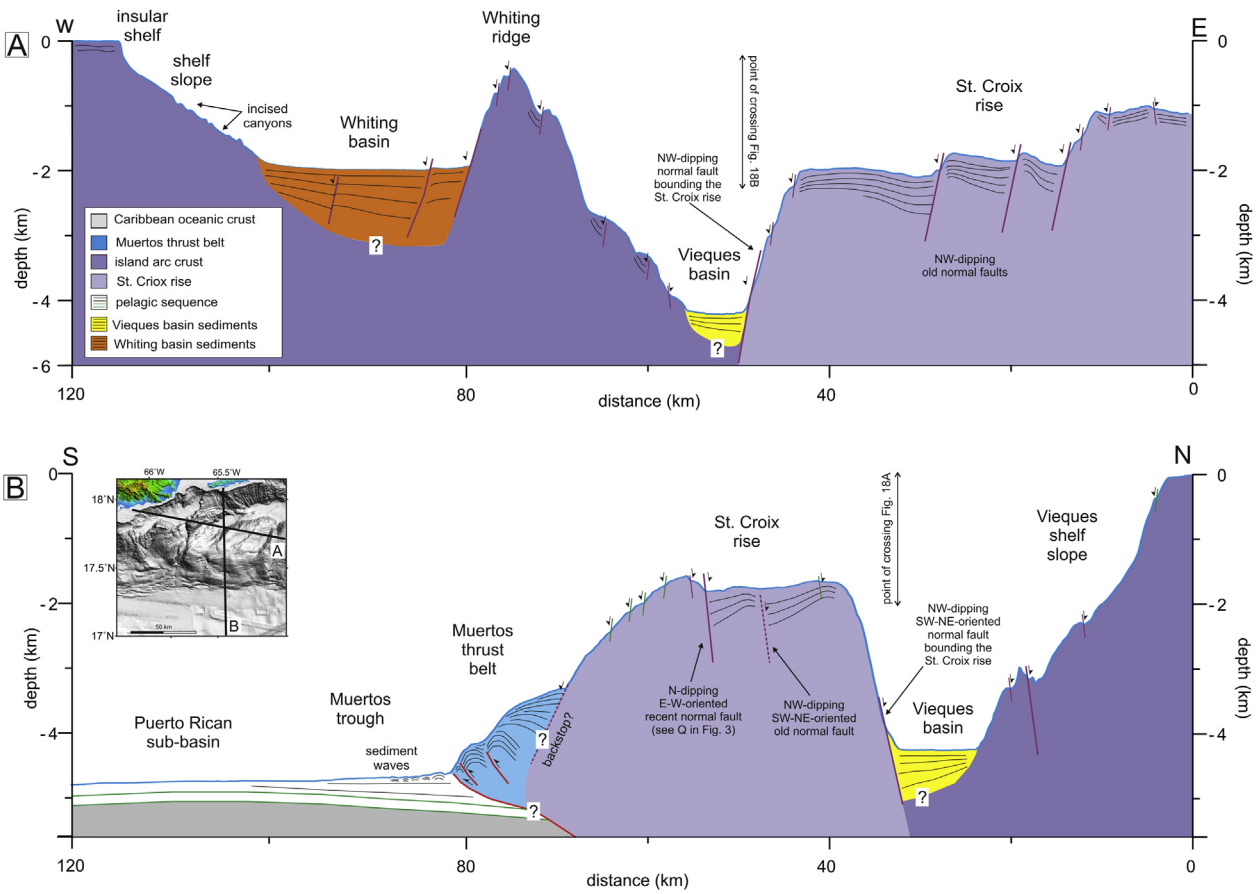

Figure 18. Schematic cross-sections deduced from this study. The bathymetric profiles were extracted from the DEM of Figure 2A. See inset map for location and Figure 4B for legend. **A)** WNW-ESE-oriented cross-section. **B)** NS-oriented cross-section.

that flanks to the east the flat-topped WNW–ESE-trending Grappler bank (≈70 mbsl; Fig. 2A) and ends in the western Whiting ridge (Fig. 3). Assuming that the NE-facing escarpment of the Grappler bank is the prolongation of the Great Southern Puerto Rico fault zone, the seismic image shows a large dip-slip fault displacement that has contributed to the formation of the Whiting basin. No strike-slip displacement can be confirmed from seismic data, but if it exists, it must be minor, and dip-slip motion is prevalent in the southeastern end of the Great Southern Puerto Rico fault zone. The Grappler bank could be a detached remnant of the Puerto Rico–Virgin Islands carbonate platform (Mann et al., 2005; Chaytor and ten Brink, 2014), and shows a flat carbonate cap of ≈0.3 sTWT of thickness with minor recent faulting (Fig. 20). Southwards of the Grappler bank, there are at least ≈0.7 sTWT of layered sedimentary beds deposited over faulted and tilted blocks. These tilted blocks seem to be the northeastern continuation of the Grappler ridge and to be present beneath the horizontal cap of the Grappler bank, though they are not observable in the seismic data. The Grappler ridge and adjoining tilted blocks seem to form part of a succession of NNE–SSW-trending tilted blocks (i.e., domino-style tectonics; McClay, 1990) arranged in echelon that extends to the Whiting ridge and to the western St. Croix rise (Figs. 3 and 18). These blocks are NE–SW-trending in the St. Croix rise but northwestward progressively rotate clockwise to be ENE–WSW-trending in the south of Grappler bank. These tilted blocks are formed by a series of S-tilted blocks and yield NE–SW-trending bathymetric ridges such as the Grappler ridge (500 mbsl), western Whiting ridge (≈450 mbsl) and the eastern Whiting ridge (≈100 mbsl) (Fig. 2A; App. A). The western and eastern Whiting ridges bound the Whiting basin and the Grappler bank in the south. Griscom and Geddes (1966) and Jany et al. (1990), based on sampling and strong magnetic anomalies, suggested that a volcanic basement underlies the ridges. The western and eastern Whiting ridges are separated by a highly-incised ≈ N–S-trending canyon (Whiting canyon; WC in Fig. 3). This canyon, which is described for the first time in the present study, starts in the Whiting basin but is disconnected from the basin seafloor by a NNW-dipping normal fault scarp that forms the north flank of the Whiting ridges (Figs. 19 and 21). This canyon could be the surface expression of an old major W-dipping normal fault (Whiting canyon fault), but sediments filling the canyon do not show fanning geometry (Fig. 23). This major fault is oblique to E–W-trending structures along the shelf slope sub-province and to the NE- and ENE-trending faults of the western Anegada passage province. It terminates downslope in a region where the upper thrust belt disappears and the width of the thrust belt is significantly reduced.

4.4.2. *Western Virgin Islands basin*

In this section we review the previous studies carried out in the western Virgin Islands basin (e.g., Jany et al., 1990; Raussen et al., 2013; Chaytor and ten Brink, 2014) and provide new observations on the shallower structure. The western Virgin Islands basin consists of an E–W-trending confined bathymetric depression (~4500 mbsl) bounded by steep walls located between the St. Croix rise and the insular shelf of Vieques island (Fig. 2A, App. A). The seafloor is composed of a major basin plain and a deeper and smaller sub-basin close to the northern bound. The major plain and the sub-basin are separated by a 60 m-high curved scarp that

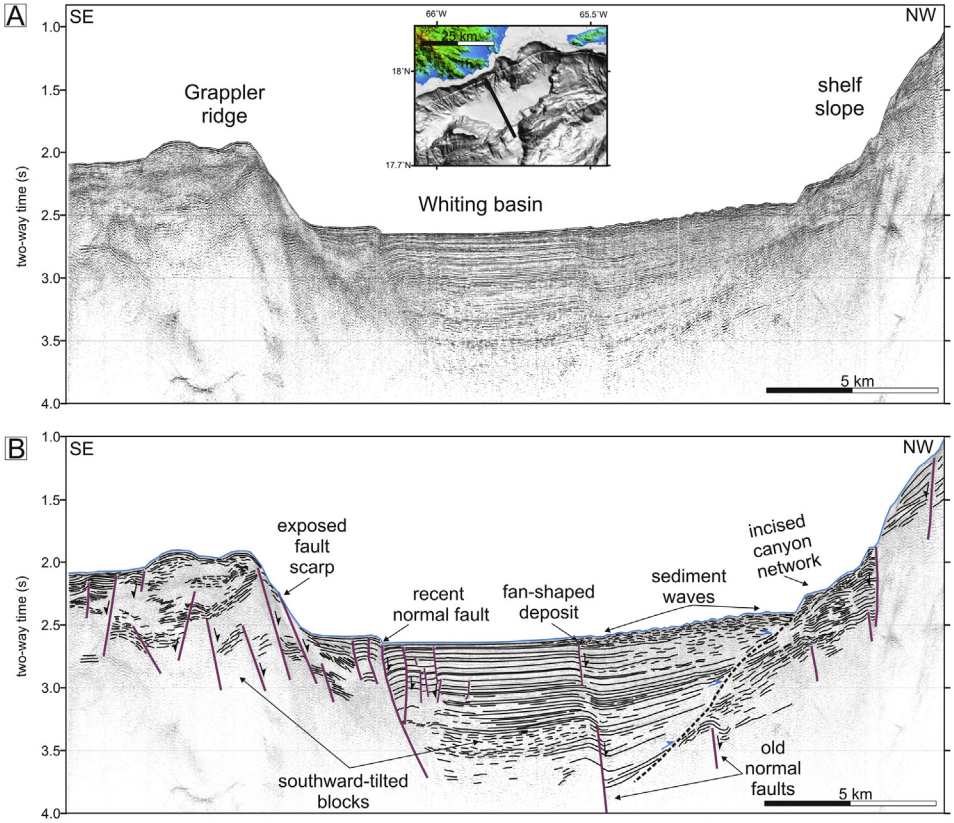

Figure 19. **A**) Post-stack migrated MCS profile. See location in the inset map. V.E. is 4.9× on the seafloor. **B)** Line drawing interpretation. See Figure 4B for legend.

extends eastward along the Whiting ridge (Fig. 3). This scarp was interpreted as an N-dipping normal fault (Chaytor and ten Brink, 2014) and also as a normal fault with a right-lateral component (Raussen et al., 2013). Westward the major basin plain becomes shallower and narrower showing an E–W-oriented bathymetric ridge that communicates with the Vieques basin. The Vieques basin is an ENE–WSW-elongated bathymetric depression (~4200 mbsl) covering an area of approximately ~125 km^2 in the western end of the Virgin Islands basin (Figs. 2A and 18). The bathymetric ridge separating the Virgin Islands and Vieques basins was interpreted to be a push-up between active left-lateral strike-slip faults (Jany et al., 1990), but it could also likely be a S-tilted block (Fig. 3). The Virgin Islands basin contains a sequence over 2.2 sTWT-thick of parallel to sub-parallel layered sediments tilted southward and buried by a 150–200 m-thick sequence of horizontally-ponded sediments (Chaytor and ten Brink, 2014). The Vieques basin contains 0.4 sTWT of horizontally-ponded sediments overlying S-tilted parallel to sub-parallel sediment beds, reflecting past movements along a N-dipping normal fault in the southern bound of the basin (Fig. 24). This stratigraphic architecture of both basins likely reflects past movements along N-dipping normal faults that are no longer active within and adjacent to the basins, forming the southern wall of the basin (Jany et al., 1990; Chaytor and ten Brink, 2014). The northern wall of the Virgin Islands basin consists of a steep slope incised by numerous canyons flowing from the edge of the Puerto Rico–Virgin Islands platform to the basin seafloor. Canyon paths are relatively straight except where they are interrupted and offset along the slope because of the existence of fault-controlled ridges (Fig. 3; Chaytor and ten Brink, 2014). Southwestward of Vieques Island, there is a large channel-canyon system with many tributaries deviated eastward (Vieques canyon; VC in Fig. 3; Chaytor and ten Brink, 2014). At the base of the shelf slope, the Vieques canyon encounters the eastern termination of the Whiting ridge and the flow is re-directed eastward surrounding the ridge. The eastern termination of the Whiting ridge seems to be a S-tilted block that forms a S-facing scarp towards the Vieques basin with frequent slope failures (Figs. 3 and 18). Where the ridge is smaller, the channel-canyon system debouches in the northeastern corner of the Vieques basin. This channel-canyon system seems to be the only channelized turbidite supply to the Vieques basin, which contains at least 1 sTWT of sediment thickness (Fig. 24). To the southwest of the Vieques basin is located the Jungfern passage where the entrance of the Atlantic currents into the Caribbean interior takes place (JP in Figs. 2A and 3).

4.4.3. *Western St. Croix rise*

The St. Croix rise is an E–W-trending bathymetric high, 150 km-long and 55 km-wide, where the St. Croix Island is located (SCR in Fig. 1). This rise shows marked morphostructural differences between the northern and southern flanks, and along strike (Fig. 18). The northern flank is sinuous and steep showing gradients on average >20°, and locally >40°, leading many investigators to suggest that this slope is the exposed scarp of a major sinuous N-dipping normal fault (e.g., Jany et al., 1990). Locally the slope shows a benched zone at ~2900 mbsl (Z in Fig. 3) that could be a faulted block controlled by the intersection of the E–W-trending faults along the northern flank and the NE–NW-trending faults in the summit of the St. Croix rise. Along the summit of the rise, there is a succession of SE-tilted blocks bounded by major normal faults that develops a domino-style tectonics (Fig. 24). The surface expression of these faults is NE–SW-trending bathymetric escarpments with occasional slope failures and slump deposits at the base. The major fault escarpment reaches a maximum height of 2200 m and forms the south-eastern bound of the Vieques basin (Fig. 3). The domino-

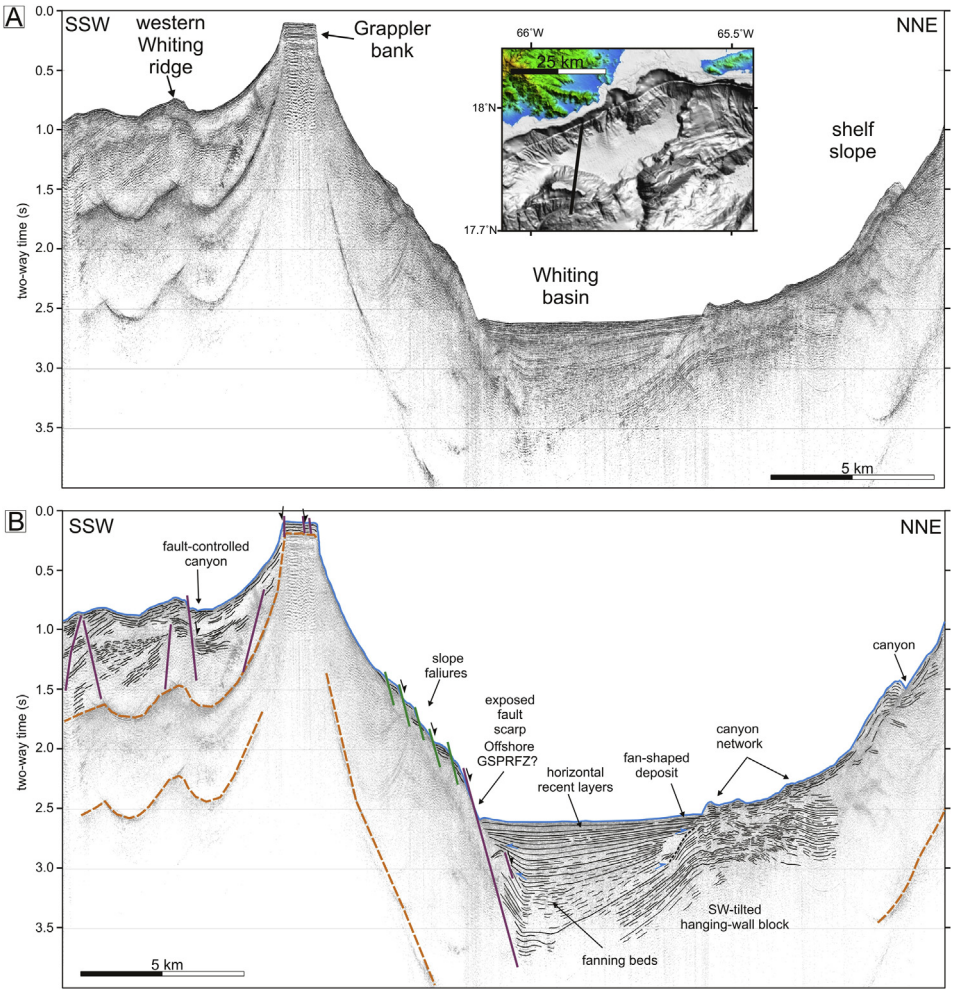

Figure 20. **A**) Post-stack migrated MCS profile. See location in the inset map. V.E. is 6.0× on the seafloor. **B)** Line drawing interpretation. See Figure 4B for legend. GSPRFZ = Great southern Puerto Rico fault zone.

style tectonics has yielded a succession of benches that become deeper to the northwest and end in the E–W- to SW–NE-oriented fault-controlled northern flank of the St. Croix rise (Fig. 18A). The top of the St. Croix rise is covered by asymmetric sedimentary wedges of at least 1 sTWT of thickness that show closely-spaced old faulting (Fig. 24). The SE-tilting of the blocks seems to be inactive because there are recent horizontally-ponded sediment beds of 0.2 sTWT of thickness lying unconformably over the asymmetric sedimentary wedges. The NE–SW-trending inactive domino structure terminates southward in a 080°-trending fault (Q in Fig. 3). This fault can be outlined along 55 km and shows a N-facing scarp with a maximum height of 350 m that loses bathymetric expression eastward. Old SCS data crossing the fault do not have enough resolution to study the possible recent activity (USGS cruise in Fig. 2B). The southern flank of the St. Croix rise is characterized by a steep but continuous slope largely devoid of channelized features (Fig. 2A). Only two channelized features are observable: the Fredericksted canyon flowing from the summit of the St. Croix rise (FC in Fig. 3; Holcombe, 1979) and another unnamed canyon (W in Fig. 3) flowing along the valley formed by the 080°-trending fault (Q in Fig. 3). In the western end of this fault, the canyon turns sharply southwards along the southern flank. This southern flank is covered by slope sediments and characterized by frequent active slope instabilities. At the base of the flank, there is a narrow deformed belt which is the eastward continuation of the Muertos thrust belt (see Section 4.2.1; Fig. 18B).

5. Discussion

5.1. Kinematics of the Investigator fault zone

Researchers have proposed that the Investigator fault zone could be a major active strike-slip fault that accommodates left-lateral slip related to an oblique convergence at the Muertos thrust belt (van Gestel et al., 1998; Mann et al., 2005). Based on low resolution bathymetric data, LaForge and McCann (2005) suggested the existence of two distinct sectors separated at 66.4°W. They did not interpret the Jaguey spur as a part of the Investigator fault zone. To the west of 66.4°W (the central sector proposed in the present study) they suggested a predominant left-lateral strike-slip motion, while to the east of 66.4°W (the eastern sector proposed in the present study) they suggested left-lateral strike-slip and an increased normal component. The offsets between the different sectors accommodated by relay ramps were formerly interpreted as NW–SE-trending right-lateral strike-slip faults associated with the dominant tectonics of the Great Southern Puerto Rico fault zone (Jany et al., 1990). Strike-slip motion in the Investigator fault suggests a NE–SW-trending oblique convergence between the

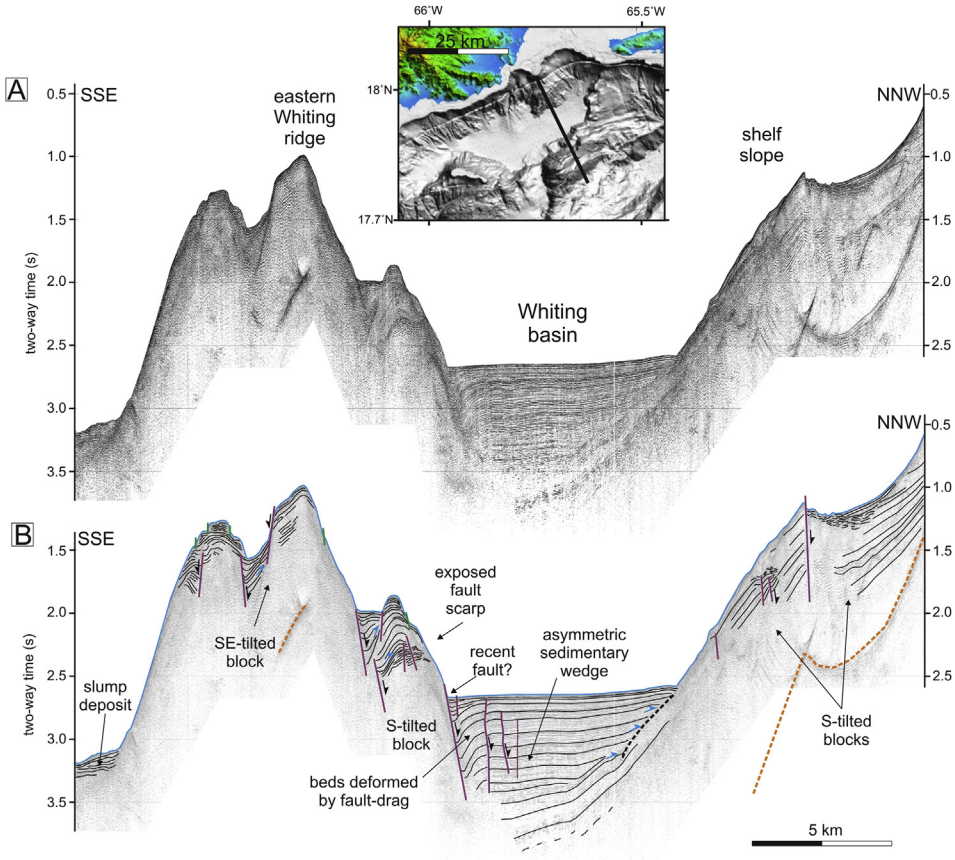

Figure 21. **A**) Post-stack migrated MCS profile. See location in the inset map. V.E. is 6.0× on the seafloor. **B)** Line drawing interpretation. See Figure 4B for legend.

overriding island arc and the Caribbean plate's interior (yellow arrows in Fig. 25). This oblique convergence would be accommodated along the Muertos margin by means of the coexistence of the subparallel Muertos thrust belt and the strike-slip Investigator fault. The coexistence of thrust belts and strike-slip faults in oblique convergent margins was commonly interpreted in other localities as a model of strain partitioning (e.g., Sumatra, McCaffrey et al., 2000; northern Hispaniola, Calais et al., 2002; Mann et al., 2002; Puerto Rico trench, ten Brink and Lin, 2004).

The oblique convergence along the Muertos trough was also inferred from the progressive eastward narrowing of the thrust belt until it disappears to the south of St. Croix (Masson and Scanlon, 1991). However, this oblique convergence has been strongly questioned by detailed observations of the deformational structures along the Muertos thrust belt south of the Mona passage and Dominican Republic (Granja Bruña et al., 2009, 2014; ten Brink et al., 2009). The Muertos thrust belt consists of an S-verging imbricate thrust system without any strike-slip faulting. In addition, numerous symmetric narrow recesses along the deformation front have been interpreted as damage zones of the imbricate structure as a result of the overthrusting of the igneous basement highs of the Caribbean plate's interior. This combination of absence of strike-slip faulting and the occurrence symmetric recesses strongly supports a southward transport direction of the Muertos thrust belt over the Caribbean plate's interior (i. e., orthogonal convergence). Sand-box kinematic analogue modeling for the northeastern Caribbean has reproduced the along strike asymmetry of the Muertos thrust belt formed by orthogonal convergence between the island arc and the Caribbean plate's interior (ten Brink et al., 2009). The cross-arc transmission of the compressive stresses yielded by the high oblique subduction at the Puerto Rico trench yields an asymmetric Muertos thrust belt in the backarc formed by orthogonal convergence. The same analogue modeling also questions the existence of strike-slip faulting coexisting with the thrust belt in the Muertos margin. The high oblique convergence at the Puerto Rico trench yields strike-slip faults along the forearc area (e.g., Bunce Fault; BF in Fig. 1). However, the strike-slip component is mainly accommodated in the forearc and interior zones of the island arc, and is not transmitted to the backarc. Therefore, orthogonal convergence does not favor the development of a strain partitioning model along the Muertos margin.

In order to evaluate the recent activity along the Investigator fault zone, we study the interaction between canyon-channel paths and the steps and slope breaks related to the activity of the major fault branch. This analysis can only be carried out in the central sector where canyon-channel paths cross-cut the surface expression of the fault formed by a bench-like feature and a smooth convex slope break. In the western and eastern sectors, the large amount of dip-slip fault motion has disconnected the drainage of the upward slope from the downslope network, and the flow is deviated along the fault trace. In the western zone of the central sector, the deeply-incised canyons cross-cut the fault trace and do not show any lateral offset (Fig. 3). Here, the surface expression of the fault is a smooth convex slope break, with minor fault-controlled steps, that is eroded by the canyons. More eastwards the main branch of the Investigator fault yields a bench-like feature that is the result of the sediment fill of an elongated valley/trough formed along the fault trace. Where canyons flowing from upward slope reach the bench, they show a sharp change in the thalweg gradient. This change in the gradient favors the deposition of a

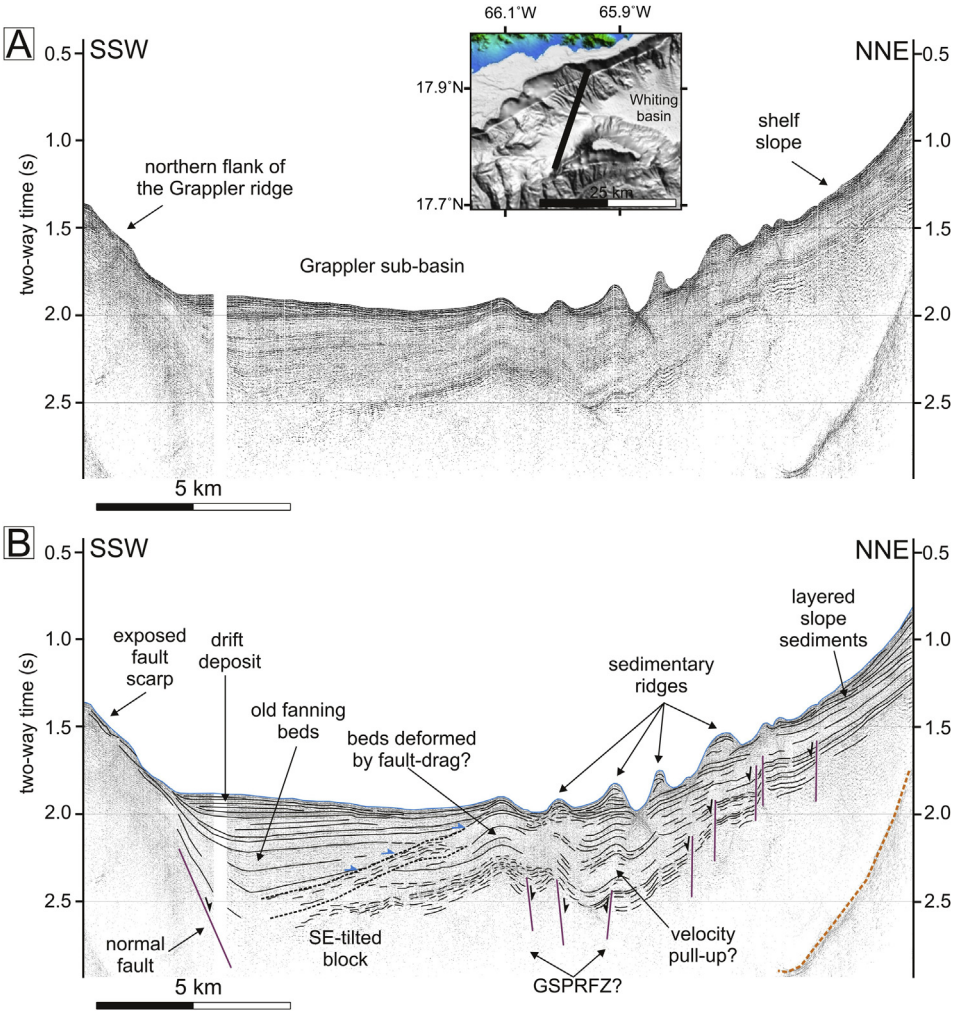

Figure 22. **A**) Post-stack migrated MCS profile. See location in the inset map. V.E. is 6.0× on the seafloor. **B)** Line drawing interpretation. See Figure 4B for legend. GSPRFZ = Great Southern Puerto Rico fault zone.

significant part of the turbiditic sediments along this valley and forms the bench-like feature. Some larger canyons erode and straightly cross-cut the bench and continue flowing downslope without any lateral offset due to potential strike-slip displacement on the fault. In the eastern termination of the central sector, the dip-slip displacement of the fault is bigger and the bench evolves to a partially sediment-filled elongated valley which canyons cannot overcome. These observations suggest that in the central sector there is predominant N–S-oriented extensional tectonics, and that while strike-slip could occur it must be insignificant and thus undetectable at the resolution of the available data. This invalidates a possible active strike-slip component along the Investigator fault zone as was speculated (e.g., van Gestel et al., 1998; LaForge and McCann, 2005). This extensional tectonics observed in the Investigator fault zone seems to be due to a stress regime observed in the top of the island arc and in the slope shelf sub-province causing the local instability of the backstop of the thrust belt. This extensional regime was widely documented in the top of the island arc (south and western coast of Puerto Rico, Mann et al., 2005; Mona passage, Grindlay et al., 2005b; Chaytor and ten Brink, 2010). In addition to this extensional regime predominating in the top of the island arc, the steep bathymetric gradients of the slope shelf sub-province strongly suggest that gravitational forces could also be involved in the extensional stress regime observed along the Investigator fault zone (i.e., slope stresses or gravitational spreading).

5.2. Deformation in the western St. Croix rise

Jany et al. (1990) proposed a two-stage evolution for the creation of the NE–SW- and E–W-trending deep basins and steep ridges of the western Anegada passage. A first NW–SE extensional event during the Eocene-Oligocene-Lower Miocene created the Virgin Islands basin and the E-tilted blocks of the St. Croix rise. A second E–W transtensional event from Pliocene to Present gave the present day pattern to this area. The western St. Croix rise shows a complex structure that attests the existence of NE–SW- and E–W-oriented normal faults. The NE–SW-trending NW-dipping normal faults observed at the summit of the rise are not active at the Present (Fig. 24). Raussen et al. (2013) interpreted the NE–SW-trending fault on the northern flank of the St. Croix rise as an active normal fault with right-lateral component but concluded that this feature could be a local structure (see Fig. 5 in Raussen et al., 2013). Our seismic data located more southwestward and transversal to this feature do not show any recent activity (Fig. 24). This is in agreement with the active NW–SE-oriented extension documented in St. Croix island from Late Miocene to Early Pliocene (Holcombe, 1979; Gill et al., 1999). These faults are cross-cut by the E–W-oriented N-dipping normal fault in the north flank and by the 080°-oriented fault in the southern zone of the summit rise (Q in Fig. 3). The NE–SW-trending faults are sub-parallel to the NE–SW-trending active structures bounding the Whiting basin and forming

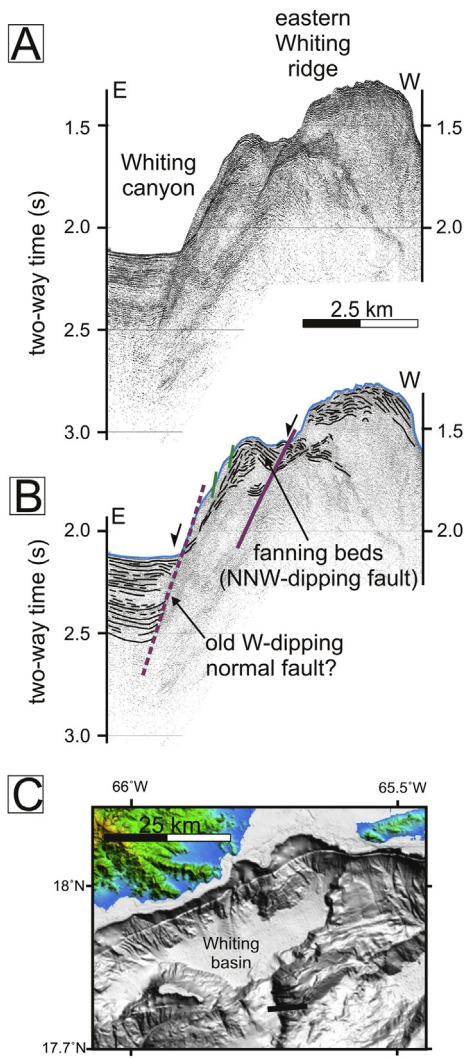

Figure 23. **A**) Post-stack migrated MCS profile. See location Figure 23C. V.E. is 4.9× on the seafloor. **B)** Line drawing interpretation. See Figure 4B for legend. **C)** Location map.

the Whiting and Grappler ridges, and also are sub-parallel to the faults observed in the insular shelf to the south of Puerto Rico (Garrison, 1969; Mann et al., 2005). The NW–SE extensional stage that affected the St. Croix rise is now inactive in this zone. This extension direction seems to be presently active only in the eastern part of the Whiting basin bounding fault (Figs. 19 and 21), perhaps in the insular shelf and southern coast of Puerto Rico (Mann et al., 2005). This fact suggests that the E–W-trending faults bounding the St. Croix rise could accommodate obliquely this active NW–SE-oriented extension, and the interior of the rise remains more stable. If this hypothesis is correct, the St. Croix rise could be explained by the first NW–SE extensional stage that formed the NE–SW-trending normal faults, while the E–W-trending faults bounding the rise become more important as the amount of extension increases and finally accommodate all of the extension at the Present. Another possibility could be that there is simply very little recent extensional activity in the western Anegada Passage province. Gill et al. (1999) proposed an average rate of 8 mm/yr in order for St. Croix Island to be placed south of Vieques Island. However, recent GPS-derived velocities show an average extensional rate of <1.5 mm/yr between St. Croix and Vieques Islands (ten Brink and López-Venegas, 2012). In addition, there are also other faults on the north wall of the Virgin Islands basin that could significantly contribute to accommodate the extensional motion, such as the possible source of the 1867 earthquake (T in Fig. 3; Barkan and ten Brink, 2010). In conclusion the St. Croix rise form part of the complex extensional fault system of the Western Anegada passage province. However, it appears decoupled from the main island arc by the E–W-trending large-dip slip faults that yielded the Virgin Island basin and then shows particular deformational features.

5.3. Active tectonic setting

The identification of recent faulting allows us to infer the existence of several active tectonic regimes in the southern Puerto Rico offshore margin (Fig. 25). In the Muertos margin there is a N–S-trending shortening/convergence regime along the Muertos thrust belt that becomes less intense eastward and seems to be insignificant or inactive to the south of St. Croix rise. Such a decrease in the convergence rate is supported by slip-rate modeling based on GPS-derived velocities and by kinematic sandbox analogue modeling. Models based on slip rate suggest a convergence of 3 mm/yr to the south of Hispaniola, decreasing to 0.2 mm/yr to the south of Puerto Rico (Benford et al., 2012). Kinematic sandbox analogue modeling also supports that the southward transmission of the compressive stresses from the subduction zone through the island arc crust to the backarc is less efficient in the Puerto Rico region than in the Hispaniola region (ten Brink et al., 2009). The development of the thrust belt undergoes major changes southwards of the Grappler bank, where the upper thrust belt (mid-slope terrace) disappears. This zone roughly coincides with the change in depth and axial slope of the Muertos trough (Apps. A and C), but we have not observed any change in the structure of the Puerto Rican sub-basin and Muertos trough province that could control the termination of the upper thrust belt. The development of the Muertos thrust belt therefore seems to be more related to the eastward decrease in convergence and the relative position of the island arc crust acting as a backstop (i.e., shelf slope sub-province) than to the structure of the incoming plate (i.e., Puerto Rican sub-basin). The insular slope is characterized by a N–S-trending extension regime evidenced along the Investigator fault zone. This N–S-trending extension could evolve northwards to the recent NW–SE-trending extension documented in the insular shelf and along the southern coast of Puerto Rico (Mann et al., 2005). In the shelf slope sub-province this N–S extension disappears in the vicinity of the Grappler bank and Whiting basin, where the NW–SE-trending extension starts to predominate. This extension is locally documented in NE–SW-trending faults along the southern basin bound and in the Grappler and Whiting ridges (Figs. 15A, 19 and 21). This extension could reactivate some dip-slip displacement in the offshore continuation of the Great Southern Puerto Rico fault zone along the eastern flank of the Grappler bank but there is no evidence of strike-slip there (Fig. 20). Active NE–SW-trending faults cut the inactive NNE–SSW-trending Whiting Canyon fault which could be a major ancient structural boundary between the Western Anegada passage and the Muertos margin provinces. The active NW–SE-trending extension seems to become less active towards the St. Croix rise because faults sub-parallel to the faults bounding the Whiting basin are inactive here (Fig. 24). The only recent deformation in the St. Croix rise could be associated with gravity-driven faults along the bathymetric scarps and with a N-dipping 080°-trending fault (Q in Fig. 3). Old SCS data are nevertheless inconclusive related to the kinematics of the 080°-trending fault (cruise with solid blue lines in Fig. 2B).

The recent deformation in the Virgin Islands basin interior has been mainly observed in a 60 m-high curved scarp near the northern bound of the basin, interpreted as a result of an active N-

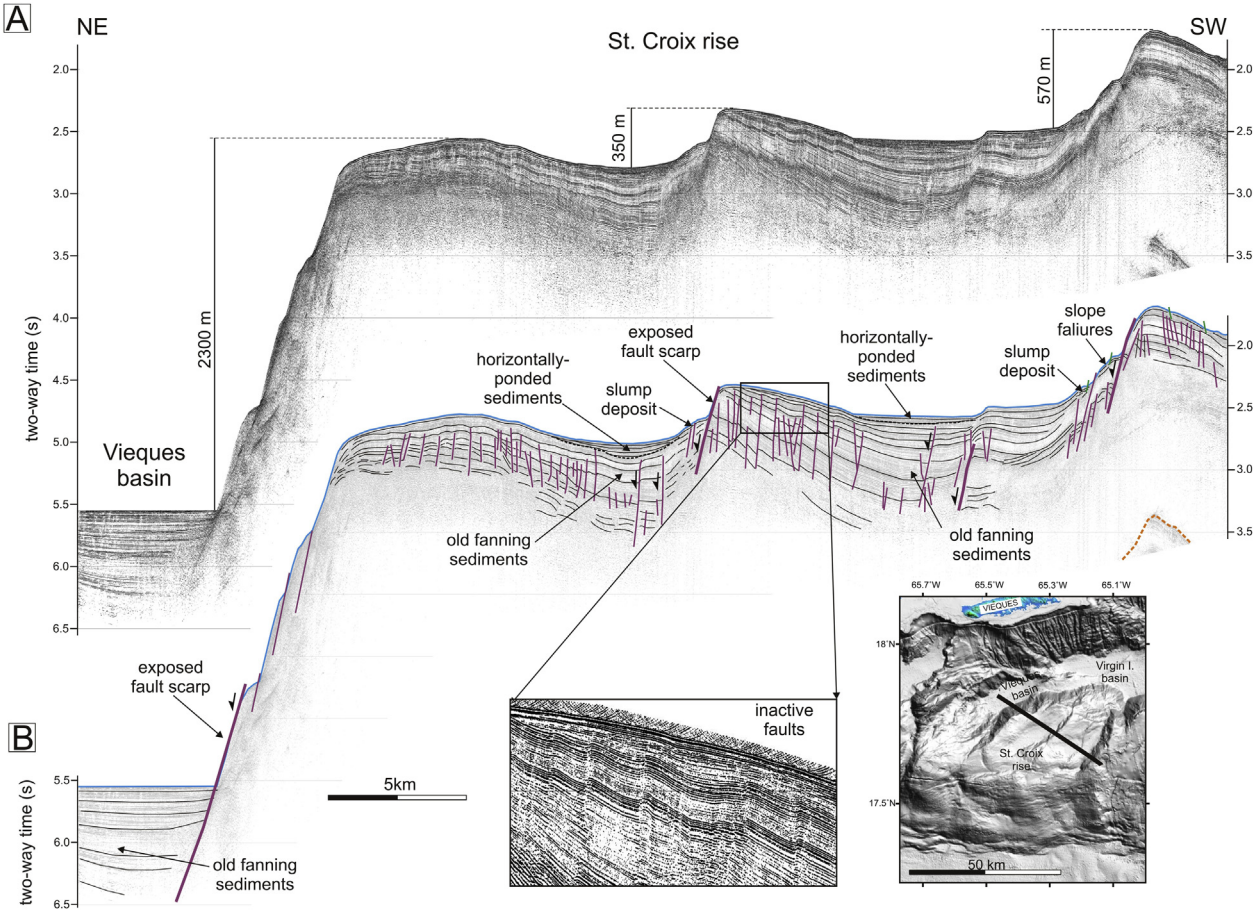

Figure 24. **A**) Post-stack migrated MCS profile. See location in the inset map. V.E. is 6.0× on the seafloor. The height of the bathymetric scarps is marked. **B)** Line drawing interpretation. See Figure 4B for legend.

dipping normal fault (Chaytor and ten Brink, 2014). This curved scarp has also been interpreted as a result of the interaction of two N-dipping normal faults with right-lateral and left-lateral components in the eastern and western terminations respectively (Raussen et al., 2013). Recent tectonic models propose a combination of N–S- to NW–SE-extension and E–W left-lateral strike-slip motion to explain the tectonic configuration of the Virgin islands basin and its vicinity (Raussen et al., 2013 and references therein). The E–W-oriented left-lateral component is supported by GPS-derived velocities giving a rate of 1.2 mm/yr between the Puerto Rico–Virgin Islands block relative to the stable part of the Caribbean plate's interior (Jansma and Mattioli, 2005). Recent GPS-derived velocities also show a ≈305°-trending average extensional rate of <1.5 mm/yr between St. Croix and the Virgin Islands (ten Brink and López-Venegas, 2012). In our study region, we have not identified any active strike-slip displacement probably because it is insignificant as is supported by the GPS data. We observe an eastward change from a NW–SE-extension in the Whiting basin to a N–S extension in the Virgin Islands basin.

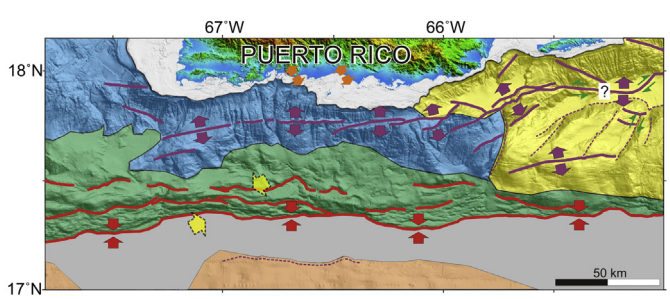

Figure 25. Map summarizing the different active tectonic regimes in the study zone. Morphotectonic provinces are color-coded as in Figure 2A. Heavier lines show main active deep-rooted faults. Dashed lines show inactive deep-rooted faults in the St. Croix rise and Puerto Rican sub-basin. Red arrows show N–S shortening. Purple arrows show N–S and NW–SE extension. Orange arrows show recent NW–SE extension documented onshore and in the insular shelf (Mann et al., 2005). Yellow arrows show oblique convergence suggested by van Gestel et al. (1998) and LaForge and McCann (2005). Green arrows show strike-slip motion in the Virgin Islands basin suggested by Raussen et al. (2013). Note that the Investigator fault zone does not show significant recent strike-slip activity and that the topography of St. Croix rise is a result of old NE–SW-trending faults cross-cut by E–W-trending faults. (For interpretation of the references to colour in this figure legend, the reader is referred to the web version of this article.)

6. Summary and conclusions

Based on along and across strike morphological, structural and sedimentological criteria, the southern Puerto Rico insular slope can be divided into four morphotectonic provinces: the Puerto Rican sub-basin and Muertos trough, the Muertos margin, the insular shelf and the western Anegada passage.

The surface expression of the Puerto Rican sub-basin and Muertos trough shows a smooth and featureless seafloor except in local zones affected by active sedimentary and tectonic processes. In the proximity of the Muertos trough, the Caribbean oceanic crust and the sedimentary section are broken over a short distance by

numerous inactive normal faults. Faults occasionally propagate the upsection deforming locally the seafloor and forming a well-preserved bathymetric scarp, but there is no evidence of recent deformation. The active deformation front is formed by the growing anticline ridges located along the base of the insular slope. Locally, the frontal fault-propagation folds are buried by horizontal beds of turbidites, suggesting that the active deformation front changed its position relative to the accretionary system over time.

The Muertos margin province shows two distinct slope sub-provinces separated by a major along-strike concave slope break: the Muertos thrust belt and the shelf slope. These two slope sub-provinces show significant along- and across-strike differences in the seafloor morphology, shallower structure and sedimentary processes:

- The Muertos thrust belt sub-province is a S-verging imbricate system formed by the accretion of pelagic and turbiditic sediments against the island arc. The surface expression of the imbricate thrust system consists of a succession of E–W-trending S-verging sub-parallel anticline ridges cored by thrust faults (i.e., fault-propagation folds). Between anticline ridges there are elongated piggy-back basins of variable size frequently showing fanning, wedge-shaped growth packages of sediments occasionally buried by horizontal sediment sequences. The Muertos thrust belt is interpreted as consisting of two thrust systems with distinct morphological and deformational styles separated by a major along-strike convex slope break: the lower thrust belt and the upper thrust belt. The major convex slope break seems to be caused by large-dip slip thrust faults that decouple the lower and upper thrust belts. The lower thrust belt occupies the base of the slope and continues eastward along the base of the slope of the St. Croix rise. The lower thrust belt shows a steep slope formed by a succession of closely-spaced small anticline ridges suggesting that the deformation is distributed in many small thrust faults. The upper thrust belt forms a mid-slope terrace with variable extension along strike that disappears eastward at approximately 66°W. The mid-slope terrace has gentler slopes formed by relatively thick blankets of slope sediments including larger perched basins and terraces burying the imbricate structure. The active deformation is mainly concentrated in local thrust faults with larger dip-slip displacements forming longer and higher anticline ridges. The progressive thickening of the slope sediment deposits, together with the vertical growth of the underlying thrust belt, contributes to form frequent gravity-driven accommodation faults favoring downslope creep processes and seaward-directed gravity flows.
- The shelf slope sub-province is a steep slope covered by a thick package of layered slope sediments highly incised by a dense canyon network. The N–S-trending flow paths are occasionally disrupted at different depths by E–W-trending fault-controlled ridges and gravity-driven failures. The Investigator fault zone is the most outstanding structural feature that dramatically changes the morphology of the slope in the shelf slope. This fault zone consists of a 130 km-long E–W-trending band of active extensional deformation which shows differential surface expression caused by along-strike changes in the magnitude and distribution of the deformation. It can be divided along strike into western, central and eastern sectors separated by relay ramps. In the eastern and central sectors, the deformation is mainly concentrated in a single S-dipping major branch fault. The eastward increase of dip-slip displacement along the major fault can be inferred from the distinct along-strike surface expression: a smooth convex slope break and a bench in the central sector and a wide and deep valley flanked by a striking ridge in the eastern sector. In the western sector the deformation is distributed in numerous normal faults over a wide band, yielding a detached bathymetric block. The activity of the fault zone and the steep slope favors the occurrence of gravity instabilities along the shelf slope. The present day pattern along the Investigator fault zone suggests that deformation is driven by a N–S-oriented extension, more intense in the eastern and western sectors, and that if there is any amount of strike-slip, it is insignificant. This extensional tectonics observed in the Investigator fault zone seems to be related to a stress regime widely observed in the top of the island arc. In the case of the slope shelf sub-province the steep bathymetric gradients strongly suggest that gravitational forces could also be involved in the extensional stress regime observed along the Investigator fault zone.

The morphology of the western Anegada passage province shows a succession of NE–SW- and E–W-trending deep basins and steep ridges representing a complex structure. The present configuration of the Whiting basin is the combined result of the intersection of several fault trends driven by a significant NW–SE-oriented extensional component: the NW–SE trend of the Great Southern Puerto Rico fault zone and the NE–SW trend of the structures dominant in the western Anegada Passage. The Whiting and Grappler ridges consist of SE-tilted blocks formed by the large displacement along N-dipping faults that make up the steep walls of the Whiting and Grappler basins. The western St. Croix rise shows a complex structure as attested by the existence of NE–SW- and E–W-oriented normal faults. The NE–SW-trending NW-dipping normal faults observed at the summit of the rise predate the E–W-bounding faults that could accommodate the extensional deformation at the Present.

The Western Anegada passage and the Investigator fault zone are characterized by extensional structures, but they are a result of distinct magnitude and distribution of the extensional deformation. The present configuration of the Western Anegada passage is a result of at least two significant phases of extension distributed in numerous NE–SW- and E–W-trending deep-rooted normal faults over a broad zone between Puerto Rico and St. Croix rise. This extensional regime has resulted the decoupling of the St. Croix rise from the Puerto Rico–Virgin Islands block and the formation of deep basins as the Virgin Islands and Vieques basins. The Investigator fault zone is a result of one phase of N–S extension observed in E–W-trending normal faults and southward tilted blocks. Although, the Investigator fault zone reflects significant changes in the magnitude and distribution of the extensional deformation, most of dip-slip is concentrated in a major branch fault. While the extension in Western Anegada passage seems to be related with a regional stress regime that has resulted in the formation of a major crustal boundary between the Puerto Rico–Virgin Islands block and the St. Croix rise-Lesser Antilles, in the Investigator fault zone the extension seems to be related with a local extensional tectonics in the top of the island arc and with the gravitational forces in the upper insular slope.

This study provides detailed observations of the shallower structure in the eastern Muertos margin and the western Anegada passage that can be used for future studies on the assessment of the natural resources and the seismic and tsunamigenic hazard in the Puerto Rico region.

Acknowledgments

This work was funded by the Spanish Ministry of Innovation and Science (Projects: REN2003-08520; CTM2006-13666 and CGL2010-17715), by the U.S. Geological Survey Coastal and Marine Geology Program (Caribbean earthquake and tsunami hazards project). We are indebted to the crew and technicians of the R/V Hespérides, R/V

Ron Brown and R/V Pelican for their professional help at sea. The professional work of the technicians of the Unidad de Tecnología Marina and U.S. Geological Survey is greatly appreciated. Old seismic profiles were provided by The Academic Seismic Portal (UTIG; Shipley et al., 2005), the National Archive of Marine Seismic Surveys (USGS), the Woods Hole Oceanographic Institution (WHOI), and the Institut Français de Recherche pour l'Exploitation de la Mer (IFREMER). We thank the National Aeronautics and Space Administration (NASA) for the SRTM90 data used in the onshore regions. We are grateful to Claudia Flores and Dave Foster for technical assistance and seismic data processing and to Bill Danforth, Brian Andrews and María Gómez Ballesteros for swath data processing. We express many thanks to L. Seeber for his helpful comments on the earlier versions of the manuscript. Some figures were drafted using free software Generic Mapping Tools (Wessel and Smith, 1998).

Appendix A. Supplementary data

Supplementary data related to this article can be found at http://dx.doi.org/10.1016/j.marpetgeo.2015.04.014.

References

Allaby, M., 2008. Dictionary of Earth Sciences, third ed. Oxford University Press, p. 654.

Andrews, B.D., ten Brink, U.S., Danforth, W.W., Chaytor, J.D., Granja Bruña, J.L., Llanes, P., Carbó-Gorosabel, A., 2014. Bathymetric Terrain Model of Puerto Rico Trench and the Northeast Caribbean Region for Marine Geological Investigations. U.S. Geological Survey Open-File Report 2013–1125. http://pubs.usgs.gov/of/2013/1125/.

Barkan, R., ten Brink, U.S., 2010. Tsunami simulations of the 1867 Virgin Islands earthquake: constraints on epicenter location and fault parameters. Bull. Seismol. Soc. Am. 100, 995–1009.

Bawiec, W.J., 1999. Geology, Geochemistry, Geophysics, Mineral Occurrences and Mineral Resource Assessment for the Commonwealth of Puerto Rico. U.S. Geological Survey Open-File Report 98–038.

Beach, D., Trumbull, J., 1981. Marine Geologic Map of the Puerto Rico Insular Shelf, Isla Caja de Muertos area. U.S. Geological Survey Miscellaneous Investigations Map I–1265.

Benford, B., DeMets, C., Calais, E., 2012. GPS estimates of microplate motions, northern Caribbean: evidence for a Hispaniola microplate and implications for earthquake hazard. Geophys. J. Int. 191, 481–490.

Bouysse, P., Baudron, J.C., Richard, M., Maury, R.C., Adreieff, P., 1985. Evolution de la terminasion nord de l'arc interne des Petites Antilles au Plio-Quaternarire. Bull. Soc. Geol. Fr. 8 I (2), 181–188.

Bowles, F., Egloff, J., 1982. Seafloor environments north St. Croix margin and Virgin Islands trough. Part 2: geology and geophysics. Nav. Ocean. Res. Dev. Act. (USA) 01–82 (26), 2.01–2.31.

Byrne, D.B., Suarez, G., McCann, W.R., 1985. Muertos Trough subduction, microplate tectonics in the northern Caribbean? Nature 317, 420–421.

Calais, E., Mazabraud, Y., Mercier de Lepinay, B., Mann, P., Mattioli, G., Jansma, P., 2002. Strain partitioning and fault slip rates in the north-eastern Caribbean from GPS measurements. Geophys. Res. Lett. 29, 1856. http://dx.doi.org/10.1029/2002GL015397.

Calassou, S., Larroque, C., Mallavieille, J., 1993. Transfer zones of deformation in thrust wedges: an experimental study. Tectonophysics 221, 325–344.

Carbó-Gorosabel, A., Córdoba, D., Martín Dávila, J., ten Brink, U., Herranz, P., Von Hilldebrandt, C., Payero, J., Muñoz Martín, A., Pazos, A., Catalán, M., Granja, J.L., Gómez, M., GEOPRICO-DO Working Group, 2005. New marine geophysical survey explores active tectonics at north-eastern Caribbean Plate Boundary. Eos Trans. Am. Geophys. Union 86 (51), 537–540.

Carbó-Gorosabel, A., Córdoba-Barba, D., Martín-Dávila, J., Granja-Bruña, J.L., Llanes Estrada, P., Muñoz-Martín, A., ten Brink, U.S., 2010. Exploring active tectonics in the Dominican Republic. Eos Trans. Am. Geophys. Union 91 (30), 261–268.

Case, J.E., Holcombe, T.L., 1980. Geologic-tectonic Map of the Caribbean Region: Reston, Virginia, USA. U. S. Geological Survey Miscellaneous Investigations Series Map I-1100, scale: 1:2.500.000.

Chaytor, J.D., ten Brink, U.S., 2010. Extension in Mona Passage, Northeast Caribbean. Tectonophysics 493 (1–2), 74–92.

Chaytor, J.D., ten Brink, U.S., 2014. Event sedimentation in low-latitude deep-water carbonate basins, Anegada passage, northeast Caribbean. Basin Res. 1–26. http://dx.doi.org/10.1111/bre.12076.

Davis, D., Suppe, J., Dahlen, F.A., 1983. Mechanics of fold-and-thrust belts and accretionary wedges. J. Geophys. Res. 88 (B2), 1153–1172. http://dx.doi.org/10.1029/JB088iB02p01153.

DeMets, C., Gordon, R.G., Argus, D.F., 2010. Geologically current plate motions. Geophys. J. Int. 181, 1–80. http://dx.doi.org/10.1111/j.1365-246X.2009.04491.x.

Denning, W., 1955. Preliminary results of geophysical exploration for oil and gas on the south coast of Puerto Rico: Commonwealth of Puerto Rico Economic Development Administration Division, Mineralogy and Geology. Bulletin 2, 17.

Diebold, J.B., Stoffa, P.L., Buhl, P., Truchan, M., 1981. Venezuelan Basin crustal structure. J. Geophys. Res. 86 (B9), 7901–7923.

Diebold, J.B., Driscoll, N.W., EW9501 Team, 1999. New insights on the formation of the Caribbean basalt province revealed by multichannel seismic images of volcanic structures in the Venezuelan Basin. In: Hsü, K.J. (Ed.), Caribbean Basins. In: Mann, P. (Ed.), Sedimentary Basins of the World, vol. 4. Elsevier Science, N. Y, pp. 561–589.

Dillon, W.P., Edgar, N.T., Scanlon, K.M., Coleman, D.F., 1996. A review of the tectonic problems of the strike-slip northern boundary of the Caribbean Plate and examination by Gloria. Geology United States' Seafloor: the View from GLORIA, 9, pp. 135–164.

Driscoll, N.W., Diebold, J.B., 1999. Tectonic and stratigraphic development of the eastern Caribbean: new constraints from multichannel seismic data. In: Hsü, K.J. (Ed.), Caribbean Basins. In: Mann, P. (Ed.), Sedimentary Basins of the World, vol. 4. Elsevier Science, N. Y, pp. 591–626.

Edgar, N.T., Ewing, J.I., Hennion, J., 1971. Seismic refraction and reflection in Caribbean Sea. Am. Assoc. Pet. Geol. Bull. 55, 833–870.

Edgar, N.T., Saunders, J.B., et al., 1973. Initial Reports of the Deep Sea Drilling Project, vol. 15. U. S. Govt, Washington, D. C, p. 1137.

Erikson, J., Pindell, J., Larue, D., 1990. Mid-Eocene–early Oligocene sinistral transcurrent faulting in Puerto Rico associated with formation of the northern Caribbean plate boundary zone. J. Geol. 98, 365–368.

Forsthoff, G.M., Holcombe, T.L., 1983. Quaternary turbidites of Muertos Trough northeastern Caribbean sea. Composition, source and dispersal patterns. In: 10th Caribbean Geological Conference. Proceedings, pp. 353–367.

Flueh, E.R., Fisher, M.A., Bialas, J., Childs, J.M., Klaeschen, D., Kukowski, N., Parsons, T., Scholl, D., ten Brink, U., Trehu, A., Vidal, N., 1998. New seismic images of the Cascadia subduction zone from Cruise SO108-ORWELL. Tectonophysics 293, 69–84.

Fuller, C.W., Willett, S.D., Brandon, M.T., 2006. Formation of forearc basins and their influence on subduction zone earthquakes. Geology 34 (2), 65–68.

Garrison, L., 1969. Structural Geology of the Muertos Insular Shelf, Puerto Rico. U.S. Geological Survey Open-File Report no. 1270, p. 9.

Genrich, J.F., Bock, Y., McCaffrey, R., Calais, E., Stevens, C.W., Subarya, C., 1996. Accretion of the southern Banda arc to the Australian plate margin determined by global positioning system measurements. Tectonics 15 (2), 288–295. http://dx.doi.org/10.1029/95TC03850.

Gill, I., McLaughlin, P.P., Hubbard, D.K., 1999. Evolution of the Neogene Kingshill Basin of St. Croix, U.S. Virgin Islands. In: Hsü, K.J. (Ed.), Caribbean Basins. In: Mann, P. (Ed.), Sedimentary Basins of the World, vol. 4. Elsevier Science, N. Y, pp. 343–366.

Glover III, L., 1971. Geology of the Coamo Area, Puerto Rico, and its Relation to the Volcanic Arc-Trench Association. U. S. Geological Survey. Professional Paper 636, p. 102.

Granja Bruña, J.L., ten Brink, U.S., Carbó-Gorosabel, A., Muñoz-Martín, A., Gómez Ballesteros, M., 2009. Morphotectonics of the central Muertos thrust belt and Muertos Trough (northeastern Caribbean). Mar. Geol. 263, 7–33. http://dx.doi.org/10.1016/j.margeo.2009.03.010.

Granja Bruña, J.L., Muñoz-Martín, A., ten Brink, U.S., Carbó-Gorosabel, A., Llanes Estrada, P., Córdoba-Barba, D., Martín-Dávila, J., Catalán Morollón, M., 2010. Gravity modelling of the Muertos Trough and tectonic implications (NE Caribbean). Mar. Geophys. Res. 31 (4), 263–283. http://dx.doi.org/10.1007/s11001-010-9107-8.

Granja Bruña, J.L., Carbó-Gorosabel, A., Llanes Estrada, P., Muñoz-Martín, A., ten Brink, U.S., Druet, M., Gómez Ballesteros, M., Pazos, A., 2014. Morphostructure at the junction between the Beata ridge and the Greater Antilles island arc (offshore Hispaniola southern slope). Tectonophysics 618, 138–163. http://dx.doi.org/10.1016/j.tecto.2014.02.001.

Grindlay, N.R., Mann, P., Dolan, J.F., van Gestel, J.-P., 2005a. Neotectonics and subsidence of the northern Puerto Rico-Virgin Islands margin on response to the oblique subduction of high-standing ridges. In: Mann, P. (Ed.), Active Tectonics and Seismic Hazards of Puerto Rico, the Virgin Islands, and Offshore Areas. Geological Society of America, pp. 31–60. Special Paper 385.

Grindlay, N.R., Abrams, L.J., Del Greco, L., Mann, P., 2005b. Toward an integrated understanding of Holocene fault activity in western Puerto Rico: constraints from high-resolution seismic and side-scan sonar. In: Mann, P. (Ed.), Active Tectonics and Seismic Hazards of Puerto Rico, the Virgin Islands, and Offshore Areas. Geological Society of America, pp. 139–160. Special Paper 385.

Griscom, A., Geddes, W., 1966. Island-arc structure interpreted from aeromagnetic data near Puerto Rico and the Virgin Islands. Geol. Soc. Am. Bull. 66, 153–162.

Gulick, S.P.S., Bangs, N.L.B., Shipley, T.H., Nakamura, Y., Moore, G., Kuramoto, S., 2004. 3-D architecture of the Nankai accretionary prism's imbricate thrust zone off Cape Muroto, Japan: prism reconstruction via en echelon thrust propagation. J. Geophys. Res. 109, B02105. http://dx.doi.org/10.1029/2003JB002654.

Gutscher, M.A., Kukowski, N., Malavieille, J., Lallemand, S., 1996. Cyclical behaviour of thrust wedges: insights from high basal friction sandbox experiments. Geology 24 (2), 135–138.

Hardy, S., Duncan, C., Masek, J., Brown, D., 1998. Minimum work, fault activity and the growth of critical wedges in fold and thrust belts. Basin Res. 10 (3), 365–373.

Holbrook, W.S., Lizarralde, D., McGeary, S., Bangs, N., Diebold, J., 1999. Structure and composition of the Aleutian island arc and implications for continental crustal growth. Geology 27, 31–34.
Holcombe, T.L., 1979. Geomorphology and sub-surface geology west of St. Croix, U. S. Virgin Islands. In: Watkins, J.S., Montaderr, L., Dickerson, P.W. (Eds.), Geological and Geophysical Investigations of Continental Margins, Am. Assoc. Petrol. Geol. Mem. 29, pp. 353–362.
Huérfano, V., von Hillebrandt-Andrade, C., Báez-Sánchez, G., 2005. Microseismic activity reveals two stress regimes in the southwestern Puerto Rico. In: Mann, P. (Ed.), Active Tectonics and Seismic Hazards of Puerto Rico, the Virgin Islands, and Offshore Areas. Geological Society of America, pp. 81–101. Special Paper 385.
Jansma, P.E., Mattioli, G.S., 2005. GPS results from Puerto Rico and the Virgin Islands: constraints on tectonic setting and rates of active faulting. In: Mann, P. (Ed.), Active Tectonics and Seismic Hazards of Puerto Rico, the Virgin Islands, and Offshore Areas. Geological Society of America, pp. 13–30. Special Paper 385.
Jany, I., 1989. Neotectonique au sud des Grandes Antilles, collision (ride de Beata, Presqu'ile de Bahoruco); subduction (fosse de Muertos); transtension (passage d'Anegada) (Ph.D. thesis). Université Pierre-et-Marie-Curie (Paris-VI), Paris, p. 306.
Jany, I., Scanlon, K.M., Mauffret, A., 1990. Geological interpretation of combined Seabeam, GLORIA and seismic data from Anegada Passage (Virgin Islands, north Caribbean). Mar. Geophys. Res. 12 (3), 173–196.
Kopp, H., Kukowski, N., 2003. Backstop geometry and accretionary mechanics of the Sunda margin. Tectonics 22 (6), 1072. http://dx.doi.org/10.1029/2002TC001420.
Kroehler, M.E., Mann, P., Escalona, E., Christeson, G.L., 2011. Late Cretaceous-Miocene diachronous onset of back thrusting along the South Caribbean deformed belt and its importance for understanding processes of arc collision and crustal growth. Tectonics 30 (6), 1–31. http://dx.doi.org/10.1029/2011TC002918.
Kukowski, N., Schillhorn, T., Huhn, K., von Rad, U., Husen, S., Flueh, E.R., 2001. Morphotectonics and mechanics of the central Makran accretionary wedge off Pakistan. Mar. Geol. 173, 1–19.
Ladd, W.J., Worzel, J.L., Watkins, J.S., 1977. Multifold Seismic Reflections Records from the Northern Venezuela Basin and the North Slope of Muertos Trench. Marine Science Institute. University of Texas, pp. 41–56.
Ladd, J.W., Shih, Tai-Chang, Tsai, C.J., 1981. Cenozoic tectonics of central Hispaniola and adjacent Caribbean Sea. Am. Assoc. Pet. Geol. Bull. 65, 466–489.
LaForge, R.C., McCann, W.R., 2005. A seismic source model for Puerto Rico, for use in probabilistic ground motion hazard analysis. In: Mann, P. (Ed.), Active Tectonics and Seismic Hazards of Puerto Rico, the Virgin Islands, and Offshore Areas. Geological Society of America, pp. 223–248. Special Paper 385.
Lagabrielle, Y., Pelletier, B., Cabioch, G., Regnier, M., Calmant, S., 2003. Coseismic and long-term vertical displacement due to back arc shortening, central Vanuatu ; offshore and onshore data following the Mw 7.5, 26 November 1999 Ambrym earthquake. J. Geophys. Res. 108 (B11) http://dx.doi.org/10.1029/2002JB002083.
Larue, D.K., Ryan, H.F., 1998. Seismic reflection profiles of the Puerto Rico Trench: shortening between the North American and Caribbean plates. In: Lidiak, E.G., Larue, D.K. (Eds.), Tectonics and Geochemistry of the Northeastern Caribbean. Geological Society of America, pp. 193–210. Special Paper 322.
Lohrmann, J., Kukowski, N., Adam, J., Oncken, O., 2003. The impact of analogue material properties on the geometry, kinematics, and dynamics of convergent sand wedges. J. Struct. Geol. 25 (10), 1691–1711.
López-Venegas, A.M., ten Brink, U.S., Geist, E.L., 2008. Submarine landslide as the source for the October 11, 1918 Mona Passage tsunami: observations and modeling. Mar. Geol. 254, 35–46.
McCaffrey, R., Zwick, P.C., Bock, Y., Prawirodirdjo, L., Genrich, J.F., Stevens, C.W., Puntodewo, S.S.O., Subarya, C., 2000. Strain partitioning during oblique plate convergence in northern Sumatra: geodetic and seismologic constraints and numerical modeling. J. Geophys. Res.-Solid Earth 105, 28363–28376.
Marques, F.O., Cobbold, P.R., 2002. Topography as a major factor in the development of arcuate thrust belts; insights from sandbox experiments. Tectonophysics 348 (4), 247–268.
McClay, K.R., 1990. Extensional fault systems in sedimentary basins: a review of analogue model studies. Mar. Pet. Geol. 7 (3), 206–233.
McClay, K.R., 1992. Glossary of thrust tectonics terms. In: McClay, K.R. (Ed.), Thrust Tectonics. Chapman and Hall, pp. 419–434.
Manaker, D., Calais, E., Freed, A., Ali, T., Przybylski, P., Mattioli, G.S., Jansma, P.E., Pre'petit, C., deChabalier, J.-B., 2008. Interseismic plate coupling and strain partitioning in the Northeastern Caribbean. Geophys. J. Int. 174 (3), 889–903.
Mann, P., Taylor, F.W., Edwards, R.L., Ku, T.L., 1995. Actively evolving microplate formation by oblique collision and sideways motion along strike-slip faults: an example from north-western Caribbean plate margin. Tectonophysics 246, 1–69.
Mann, P., Calais, E., Ruegg, J.-C., DeMets, C., Jansma, P.E., 2002. Oblique collision in the north-eastern Caribbean from GPS measurements and geological observations. Tectonics 2 (6), 1057. http://dx.doi.org/10.1029/2001TC0011304.
Mann, P., Hippolyte, J.-C., Grindlay, N., Abrams, L.J., 2005. Neotectonics of southern Puerto Rico and offshore margin. In: Mann, P. (Ed.), Active Tectonics and Seismic Hazards of Puerto Rico, the Virgin Islands, and Offshore Areas. Geological Society of America, pp. 173–214. Special Paper 385.
Marshak, S., Wilkerson, M.S., Hsui, A.T., 1992. Generation of curved fold-thrust belts; insight from simple physical and analytical models. In: McClay, K.R. (Ed.), Thrust Tectonics. Chapman and Hall, London, pp. 83–92.
Masson, D.G., Scanlon, K.M., 1991. The neotectonic setting of Puerto Rico. Geol. Soc. Am. Bull. 103, 144–154.
Matthews, J., Holcombe, T., 1976. Possible Caribbean underthrusting of the Greater Antilles along Muertos Trough. In: Transactions of the 7th Caribbean Geological Conference. Proceedings, pp. 235–242.
Matthews, J., Holcombe, T., 1985. Venezuelan Basin of the Caribbean sea- stratigraphy and sediment distribution. Mar. Geol. 68, 1–23.
Mauffret, A., Leroy, S., 1999. Neogene Intraplate deformation of the Caribbean plate at the Beata Ridge. In: Hsü, K.J. (Ed.), Caribbean Basins. In: Mann, P. (Ed.), Sedimentary Basins of the World, vol. 4. Elsevier Science, N. Y, pp. 627–669.
Moore, G.F., Karig, D.E., 1976. Development of sedimentary basins on the lower trench slope. Geology 4, 693–697.
Moore, G.F., Shipley, T.H., Stoffa, P.L., Karig, D.E., Taira, A., Kuramoto, S., Tokuyama, H., Suyehiro, K., 1990. Structure of the Nankai Trough accretionary zone from multichannel seismic reflection data. J. Geophys. Res. 95 (B6), 8753–8765.
Mullins, H.T., Hine, A.C., 1989. Scalloped bank margins: beginning of the end for carbonate platforms? Geology 17, 30–33.
Park, J.O., Tsuru, T., Kodaira, S., Cummins, P.R., Kaneda, Y., 2002. Splay fault branching along the Nankai subduction zone. Science 297 (5584), 1157–1160. http://dx.doi.org/10.1126/science.1074111.
Raussen, S., Lykke-Andersen, H., Kuijpers, A., 2013. Tectonics of the Virgin Islands Basin, north eastern Caribbean. Terra Nova 25 (3), 252–257.
Scholl, D., von Henue, R., Vallier, T., Howell, D., 1980. Sedimentary masses and concepts about tectonic processes at underthrust ocean margins. Geology 8, 564–568.
Shipley, T., Gahagan, L., Johnson, K., Davis, M. (Eds.), 2005. Seismic Data Center. University of Texas Institute for Geophysics. www.ig.utexas.edu/sdc/.
Smith, W.H.F., Sandwell, D.T., 1997. Global seafloor topography from satellite altimetry and ship depth soundings. Science 277, 1957–1962.
Smith, G., McNeill, L., Henstock, T.J., Bull, J., 2012. The structure and fault activity of the Makran accretionary prism. J. Geophys. Res. 117, B07407. http://dx.doi.org/10.1029/2012JB009312.
Taylor, L.A., Eakins, B.W., Carignan, K.S., Warnken, R.R., Sazonova, T., Schoolcraft, D.C., 2008. Digital elevation models of Puerto Rico: procedures, data sources and analysis. NOAA Technical Memorandum NESDIS NGDC- 13, p. 27.
Trias, J., 1991. Marine Geologic Map of the Puerto Rico Insular Shelf-Guanica to Ponce Area. U.S. Geological Survey Miscellaneous Investigations Series Map I-2263, scale 1:40.000.
ten Brink, U.S., Danforth, W., Polloni, C., Andrews, B., Llanes, P., Smith, S., Parker, E., Uozumi, T., 2004. New sea floor reveals the structure of the Puerto Rico. Trench and helps assess earthquake and tsunami hazards in the Northeast Caribbean. Eos Trans. Am. Geophys. Union 85 (37), 349–354.
ten Brink, U.S., Lin, J., 2004. Stress interaction between subduction earthquakes and forearc strike-slip faults: modeling and application to the northern Caribbean plate boundary. J. Geophys. Res. 109, B12310. http://dx.doi.org/10.1029/2004JB003031.
ten Brink, U.S., 2005. Vertical motions in the Puerto Rico Trench and Puerto Rico and their cause. J. Geophys. Res. 100, B06404. http://dx.doi.org/10.1020/2004JB003459.
ten Brink, U.S., Marshak, S., Granja Bruña, J.L., 2009. Bivergent thrust wedges surrounding island arcs: insights from observations and sandbox models of the northeastern Caribbean plate. Geol. Soc. Am. Bull. 121 (11/12), 1522–1536. http://dx.doi.org/10.1130/B26512.1.
ten Brink, U.S., López-Venegas, A., 2012. Plate interaction in the NE Caribbean subduction zone from continuous GPS observations. Geophys. Res. Lett. 39, L10304. http://dx.doi.org/10.1029/2012GL051485.
Underwood, M.B., 1991. Submarine canyons, unconfined turbidite currents, and sedimentary bypassing of forearc region. Rev. Aquat. Sci. 4 (2–3), 149–200.
Underwood, M.B., Moore, G.F., 1995. Trenches and trench-slope basins. In: Busby, C.J., Ingersoll, R.V. (Eds.), Tectonics of Sedimentary Basins. Blackwell Scientific Publishers, pp. 179–219.
Underwood, M.B., Moore, G.F., 2011. Evolution of sedimentary environments in the subduction zone of southwest Japan: recent results from the NanTroSEIZE Kumano transect. In: Busby, Azor (Eds.), Tectonics of Sedimentary Basins: Recent Advances, pp. 310–326.
van Gestel, J.-P., Mann, P., Grindlay, N.R., Dolan, J.F., 1998. Structure and tectonics of the upper Cenozoic Puerto Rico-Virgin Islands carbonate platform as determined from seismic reflection studies. J. Geophys. Res. 103 (B12), 30505–30530.
von Huene, R., Scholl, D.W., 1991. Observations at convergent margins concerning sediment subduction, subduction erosion, and the growth of continental crust. Rev. Geophys 29 (3), 279–316. http://dx.doi.org/10.1029/91RG00969.
Wessel, P., Smith, W.H.F., 1998. New improved version of Generic Mapping Tools released. Eos, Trans. Am. Geophys. Union 79 (47), 579.
Willett, S., Beaumont, C., Fullsack, P., 1993. Mechanical model for the tectonics of doubly vergent compressional orogens. Geology 21 (4), 371–374.
Wynn, R.B., Stow, D.A.V., 2002. Classification and characterization of deep-water sediment waves. Mar. Geol. 192, 7–22.